Gondwana Research 81 (2020) 1–20

Contents lists available at ScienceDirect

Gondwana Research

journal homepage: www.elsevier.com/locate/gr

# The Gondwanan margin in West Antarctica: Insights from Late Triassic magmatism of the Antarctic Peninsula

Joaquin Bastias [a,*], Richard Spikings [a], Alex Ulianov [b], Teal Riley [c], Alex Burton-Johnson [c], Massimo Chiaradia [a], Lukas Baumgartner [b], Francisco Hervé [d,e], Anne-Sophie Bouvier [b]

[a] Department of Earth Sciences, University of Geneva, 1205 Genève, Switzerland
[b] Institute of Earth Sciences, University of Lausanne, 1015 Lausanne, Switzerland
[c] British Antarctic Survey, High Cross, Madingley Road, Cambridge CB3 0ET, UK
[d] Departamento de Geologia, Universidad de Chile, 8370450 Santiago, Chile
[e] Carrera de Geologia, Facultad de Ingenieria, Universidad Andres Bello, 8370106 Santiago, Chile

ARTICLE INFO

*Article history:*
Received 23 May 2019
Received in revised form 14 October 2019
Accepted 15 October 2019
Available online 19 December 2019

Handling Editor: A. Festa

ABSTRACT

Triassic orthogneisses of the Antarctic Peninsula provide evidence for the Palaeozoic and Mesozoic geological evolution of southern Gondwana within Pangaea. These rocks are sporadically exposed in southeastern Graham Land and northwestern Palmer Land, although reliable geochronological, geochemical and isotopic data are sparse. We combine new geochronological (LA-ICP-MS zircon U—Pb), geochemical, and zircon (Hf, O) and whole rock isotopic (Nd, Sr and Pb) data to constrain the age and Triassic – Palaeozoic tectonic setting of these rocks. Zircon cores record Palaeozoic arc magmatism between 253 ± 2 and 528 ± 6 Ma, which was mainly located to the west of the Eastern Palmer Land Shear Zone (Central Domain; Vaughan and Storey, 2000). The arc is considered to be an extension of contemporaneous Palaeozoic arcs that have been identified along the Pacific margin of South America and the Thurston Island Block. Regions to the east of the Palmer Land Shear Zone (Eastern Domain, Vaughan and Storey, 2000) were located distal from the Terra Australis Margin, and possibly resided within Sunsas-aged belts within Pangaea. Triassic continental arc, calc-alkaline magmatism during 223–203 Ma modified the crust of the Antarctic Peninsula on both sides of the Eastern Palmer Land Shear Zone. Magmatic sources included igneous and sedimentary crustal material, which formed by crustal reworking during Sunsas- and Braziliano-aged orogenesis, and Palaeozoic arc magmatism. Arc magmatism accompanied sinistral extension which brought both domains into the arc and resulted in steady oceanward migration of the Triassic arc during the Middle – Late Triassic. We propose that sinistral displacement occurred along the Eastern Palmer Land Shear Zone, and this structure was active as early as the Triassic. Finally, we conclude that both the Eastern and Central Domains are autochthonous to Gondwana.



## 1. Introduction

West Antarctica is considered to be composed of an amalgamation of several continental blocks, including the Antarctic Peninsula block, which were originally dispersed along the southern margin of Gondwana, and have affinities with South America, Zealandia and southern Africa (Fig. 1; Storey et al., 1998; Dalziel and Elliot, 1982). The West Antarctic blocks were located along the Terra Australis margin of Cawood (2005), where proto-Pacific oceanic lithosphere was subducted along the west coast of South America, southern Africa, East Antarctica, and fragments of what are now West Antarctica, Zealandia and the east coast of Australia (Fig. 1). Rifting of South America, Africa, East Antarctica, India, Australia and Zealandia drove crustal block translations and rotations that lead to the breakup of Gondwana and the assembly of West Antarctica (e.g. Grunow et al., 1987, 1991). The primary aim of this work is to improve reconstructions of the Antarctic Peninsula within the Terra Australis margin, and thus advance our understanding of the configuration of southern Gondwana, and the disassembly of Pangaea, which commenced in the Triassic (e.g. Golonka and Bocharova, 2000; Spikings et al., 2016).

The proto-Antarctic Peninsula was flanked by Patagonia, East Antarctica and the remainder of the West Antarctic terranes during the late Palaeozoic and Mesozoic (e.g. Riley et al., 2017a; Fig. 1). However, extensive ice coverage and geographic remoteness has led to a paucity of quantitative data from West Antarctic blocks that could constrain their histories within Gondwana, their subsequent disassembly and re-amalgamation to form West Antarctica. We present new geochronological (zircon U—Pb dates obtained using LA-ICPMS; Laser Ablation – Inductively Coupled Mass Spectrometry), geochemical (whole

* Corresponding author.
*E-mail address:* joaquin.bastias@unige.ch (J. Bastias).

https://doi.org/10.1016/j.gr.2019.10.018
1342-937X/

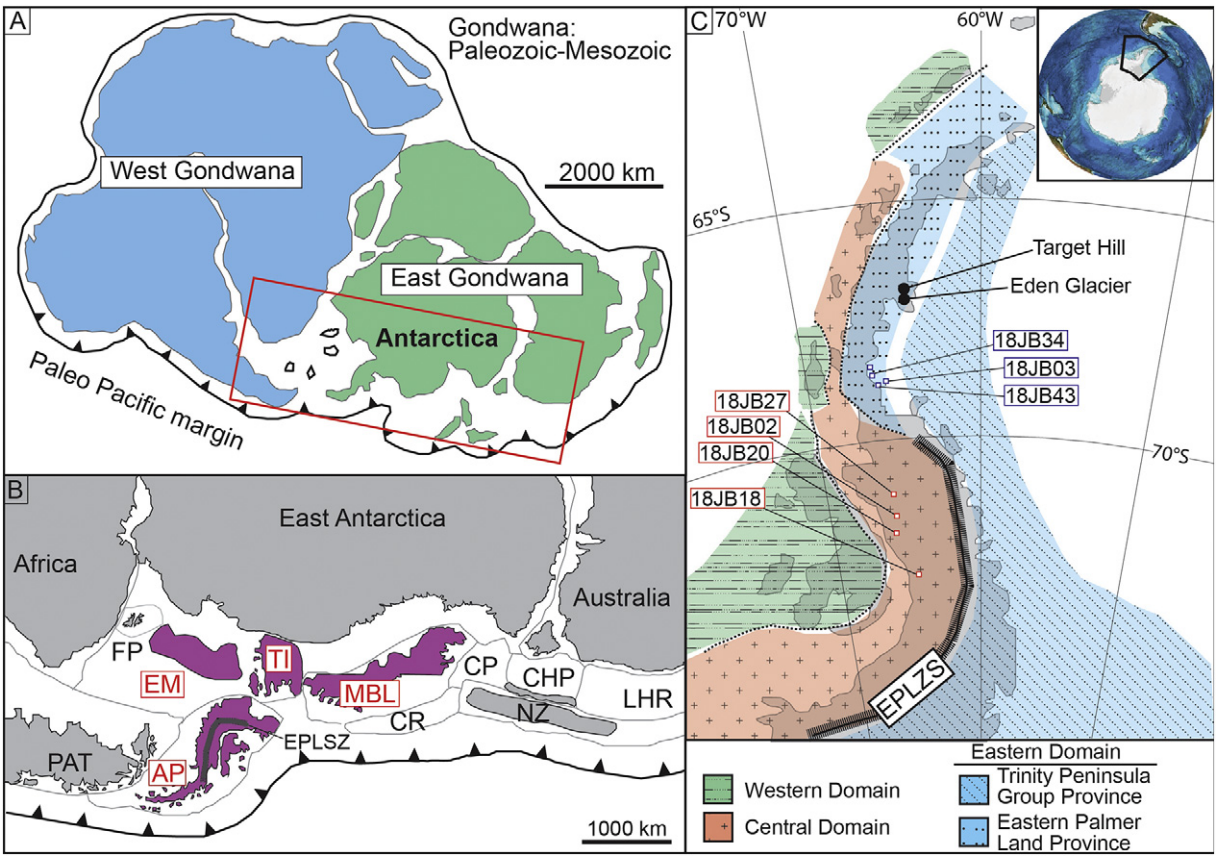


**Fig. 1.** (A) Palaeogeographic reconstruction of Palaeozoic–Mesozoic Gondwana showing the active paleo–Pacific margin (from Meert and Lieberman, 2008; Nelson and Cottle, 2017, 2018). (B) Reconstruction of West Antarctic blocks (in purple) along the Gondwanan plate margin during the late Palaeozoic–early Mesozoic (Elliot, 2013). (C) Map of the present day Antarctic Peninsula showing the locations of the Western, Central and Eastern domains, and the Eastern Palmer Land Shear Zone of Vaughan and Storey (2000). Locations and labels of Triassic crystalline rocks are also shown. AP: Antarctic Peninsula, CHP: Challenger Plateau and West New Zealand, CP: Campbell Plateau, CR: Chatham Rise, EPLSZ: Eastern Palmer Land Shear Zone, PAT: Patagonia, FP: Falkland Plateau, LHR: Lord Howe Rise, MBL: Marie Byrd Land, NZ: East New Zealand, TI: Thurston Island.

rock) and isotopic (whole rock Nd, Sr, Pb; zircon Hf and O) data acquired from Triassic igneous units exposed in the Antarctic Peninsula (Graham and Palmer Land, Fig. 2). The igneous rocks are mainly orthogneisses that crop out in remote locations that were i) sampled during two field seasons as part of this study, and ii) were provided from the British Antarctic Survey archive collection. We combine our data with comparable datasets from the Antarctic Peninsula (Flowerdew et al., 2006; Hervé et al., 2006a; Bastias and Hervé, 2013; Castillo et al., 2016; Nelson and Cottle, 2017; Riley et al., 2017a), South America (Castillo et al., 2017; Hervé et al., 2016; van der Lelij et al., 2018; Mišković and Schaltegger, 2009) and Thurston Island (Nelson and Cottle, 2017; Riley et al., 2017b). These data are used to constrain the geological evolution of rocks of the Antarctic Peninsula during the breakup of southern and western Gondwana, and the subsequent assembly of West Antarctica. Similar analytical techniques have been used by other studies (e.g. Kemp et al., 2009; Cochrane et al., 2014; Spikings et al., 2015; Nelson and Cottle, 2018; Augustsson et al., 2016; Balgord, 2017) to investigate the tectonic histories of crustal blocks along the Terra Australis margin.

Previous geochronological studies from the Antarctic Peninsula (e.g. Milne and Millar, 1989; Tangeman et al., 1996; Millar et al., 2002; Clemens, 2003; Flowerdew et al., 2006; Riley et al., 2012a) identified Triassic magmatism, which incorporated abundant xenocrystic zircon cores (Flowerdew et al., 2006; Riley et al., 2012a), eluding to the presence of an older basement sequence. However, there remains a considerable degree of uncertainty regarding the tectonic setting in which the Triassic magmas were produced, the sources of their inherited cores and the implications for the late Palaeozoic – early Mesozoic geological history. While a majority of studies suggest extension prevailed in western South America (e.g. Spikings et al., 2016), Zealandia (e.g. Kula et al., 2007) and Australia (e.g. Veevers and Tewari, 1995) during the Triassic, it has recently been suggested that compression prevailed within Patagonia (Navarrete et al., 2019; Suárez et al., 2019). Nevertheless, the Triassic tectonic setting of the Antarctic Peninsula has not been explored in detail.

Early interpretations used litho-stratigraphic correlations between Patagonia and the Antarctic Peninsula to suggest that both formed part of the Late Jurassic – Early Cretaceous Andean active margin (e.g. Suarez, 1976), which is considered to have initiated during the Triassic (e.g. Coloma et al., 2017; González et al., 2018; Oliveros et al., 2018; del Rey et al., 2016). Later, Vaughan and Storey (2000) mapped a regionally extensive shear zone in Palmer Land (Eastern Palmer Land Shear Zone), and proposed that the Antarctic Peninsula developed as a result of a mid-Cretaceous collision and accretion of an allochthonous arc (Central Domain) with a former Gondwanan block (Eastern Domain; Fig. 1). This period of collision is generally referred to as the Palmer Land Event and is interpreted as the time of terrane accretion (Vaughan et al., 2012a). The same authors defined the Western Domain, which they describe as an accretionary complex (e.g. Storey and Garrett, 1985; Fig. 1). However, subsequent studies questioned the collisional model on the basis of sedimentary provenance and the isotopic composition of igneous rocks, which led to its partial revision (Vaughan et al., 2012a, 2012b) and alternative hypotheses (e.g. Riley et al., 2012b; Burton-Johnson and Riley, 2015). Burton-Johnson and Riley (2015) conducted a thorough review of the most recent dataset of the Antarctic Peninsula and presented an in-situ model for the evolution of the

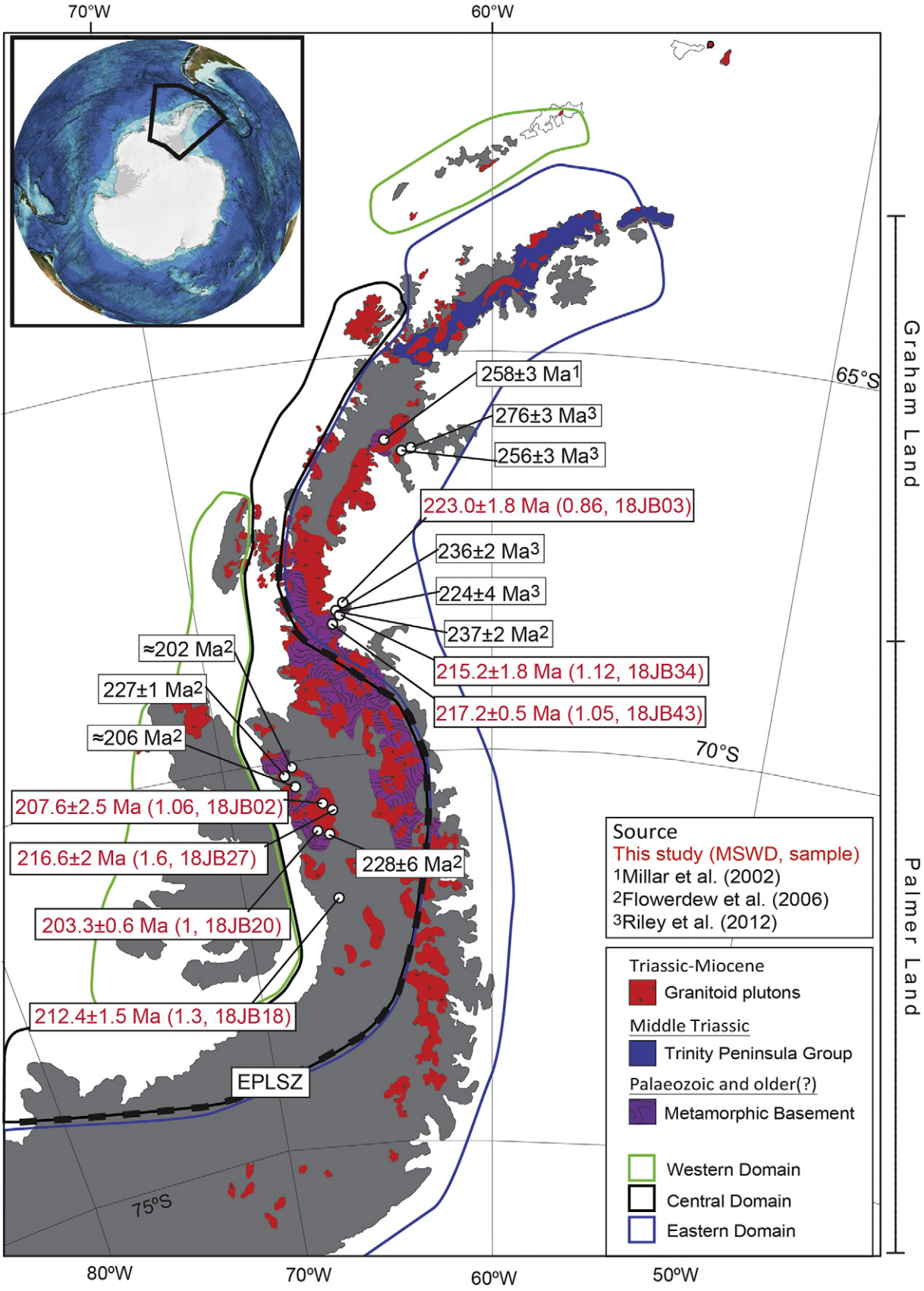


**Fig. 2.** Geological map of the Antarctic Peninsula, showing the distribution of intrusive rocks (previously referred to as the Antarctic Peninsula Batholith) and the metamorphic basement, modified from Burton-Johnson and Riley (2015). The locations of the Western, Central and Eastern domains are taken from Vaughan and Storey (2000) and Vaughan et al. (2012a). Zircon $^{206}Pb/^{238}U$ concordia ages collected in this study (in red) using LA-ICP-MS are presented along with published, pre-Jurassic U/Pb ages (in black; Millar et al., 2002; Flowerdew et al., 2006; Riley et al., 2012). All uncertainties are quoted at ±2σ. EPLSZ: Eastern Palmer Land Shear Zone, from Vaughan and Storey (2000) and Vaughan et al. (2012a).

margin, which included the initiation of subduction during the Triassic – Permian period. Triassic igneous units are exposed in both domains, and thus an analysis of their distribution, and a comparison of their crystallisation ages, geochemical and isotopic compositions will provide better constraints on the evolution of the Antarctic Peninsula.

## 2. Geological framework

### 2.1. Pre-Jurassic magmatic and metamorphic rocks

Triassic-Early Jurassic Rb—Sr whole-rock dates have been obtained from orthogneisses, granites, granodiorites and tonalites located along the east coast of Graham Land, where they range from 209 ± 3 Ma (Pankhurst, 1982) to 204 ± 6 Ma (Hole, 1988), and in eastern Palmer Land where they range between 232 ± 4 Ma and 199 ± 7 Ma (Wever et al., 1994; Scarrow et al., 1998). The cited studies interpreted the Rb—Sr dates to be accurate measurements of the time of crystallisation. More recently, zircon U—Pb geochronology of foliated Triassic orthogneisses, migmatites and granitic gneisses yielded $^{206}Pb/^{238}U$ concordia ages spanning between 236 ± 2 Ma to 224 ± 4 in two localities along the east coast of Graham Land in the Eastern Domain (Fig. 2; Flowerdew et al., 2006; Riley et al., 2012a), and between 227 ± 1 and ~202 Ma in northwestern Palmer Land in the Central Domain (Fig. 2; Flowerdew et al., 2006). Inherited zircon cores in the Triassic plutons yield Carboniferous, Permian and Middle Devonian concordia ages, which are attributed to periods of high-temperature metamorphism and magmatism (Millar et al., 2002; Flowerdew et al., 2006). These Triassic rocks are peraluminous and yield whole rock $^{87}Sr/^{86}Sr_i$ ratios of 0.705 to 0.721 (Wever et al., 1995; Scarrow et al., 1998), suggesting the magmatic source regions mainly consisted of crustal components.

Geothermobarometric and geochronological analyses were used to suggest these rocks experienced a high-temperature metamorphic event during the Late Triassic – early Jurassic (Flowerdew et al., 2006; Millar et al., 2001, 2002; Leat et al., 1995; Wever et al., 1994; Scarrow et al., 1998). We refer to these outcrops as local crystalline basement because they are the oldest exposed rocks that have been dated in the sampled region. However, it is likely that most of these siliceous units formed by partial melting of pre-existing crust, which may not be locally exposed. These Triassic intrusive units could be grouped into the informal term "Antarctic Peninsula Batholith" which is frequently used in the Antarctic Literature (e.g. Leat et al., 1995). However, we choose to not use that division because it is poorly defined with respect to time, and encompasses rocks that span from the Tertiary to the Mesozoic. Rather, we use the term "Rymill Granite Complex" to describe Triassic orthogneisses exposed in the Central and Eastern Domains of the Antarctic Peninsula. Mainly undifferentiated, high-grade, deformed metamorphic rocks are grouped as the Metamorphic Basement (Fig. 2) to the intrusive units. Geochronological analyses are limited to Target Hill and Eden Glacier, where Carboniferous metamorphism of a Devonian igneous protolith is recorded (Graham Land; Fig. 1; Millar et al., 2002; Riley et al., 2012a). These are isolated localities that have been interpreted as being representative of the crystalline basement of the Antarctic Peninsula (Milne and Millar, 1989), and may be equivalent to exposures of Carboniferous metamorphic rocks in Patagonia (Pankhurst et al., 2006). However, Riley et al. (2012a) argues that it is unlikely that Target Hill represents the basement of the Antarctic Peninsula because its spatial exposure is too limited.

### 2.2. Pre-Jurassic sedimentary rocks

Pre-Jurassic sedimentary rocks are exposed across large parts of northern Graham Land (Trinity Peninsula Group; Smellie, 1991; Fig. 2), and in isolated outcrops from southwestern Palmer Land (Fitzgerald and Erehwon Beds; Laudon, 1991). Greenschist grade metasedimentary rocks of the Permian to Middle Triassic Trinity Peninsula Group were deposited in a slope-apron position (e.g. Bradshaw et al., 2012; Smellie, 1991). Lithologies of the Trinity Peninsula Group include mudstones and sandstones deposited in turbiditic flows, sourced from an active continental arc (Smellie, 1991; Castillo et al., 2015). Depositional ages were estimated using detrital zircon U—Pb concordia ages combined with fossil evidence (Thomson, 1975; Hervé et al., 2006a; Barbeau et al., 2010). These rocks host Triassic fossils and were mainly derived from a dominant Permian igneous source that may be currently located in both the Antarctic Peninsula and Patagonia (Castillo et al., 2016). Aitkenhead (1975) used sedimentological and structural arguments to suggest that the Trinity Peninsula Group may extend into the South Shetland Islands (northwest of the Antarctic Peninsula, Western Domain; Fig. 2). However, similar metasedimentary lithologies within the Miers Bluff Formation (Hervé et al., 2006a) in Livingston Island, and the Cape Wallace Beds in Low Island (Bastias et al., 2019a) are Jurassic, which does not support a chronological correlation with the mainland of the Antarctic Peninsula.

## 3. Methods

A summary of the relevant geochronological, geochemical, and all isotopic data is presented in Table 1. Detailed datasets of the geochronology, geochemical, isotopic data are presented in the data repository available in Bastias et al. (2019b).

### 3.1. Whole rock geochemistry

Representative whole rock powders were prepared using an agate mill and major and trace elements were measured using a Philips PW2400 X-Ray Fluorescence (XRF) spectrometer at the University of Lausanne, Switzerland. The NIMN, NIMG, BHVO and SY2 standards were used for quality control. Glass fused disks prepared for XRF analyses were fragmented and mounted for additional analyses of trace and rare earth elements (REE). Measurements were made using a Perkin Elmer ELAN 6100 DRC quadrupole ICP-MS, and depending on the expected enrichment within samples, either NIST SRM 610 or 612 fused glasses were used as external standards. The laser settings used for analyses were 10 Hz frequency, 140 mJ energy and 80–120 μm spot size. Blanks were measured for ~90s, after which the laser was switched on and the signal was measured for 45 s. The Sr or $Al_2O_3$ concentrations (previously determined by XRF) were used as an internal standard. Each sample was ablated 3 times, and average concentrations were calculated offline using LAMTRACE (Jackson, 2008). The uncertainties of 3 spots per sample are ±10% for rare earth elements (REE), and ± 5% for other trace elements. Whole rock compositions have been normalised to an anhydrous state in the graphical representations.

### 3.2. Sr-Nd-Pb bulk rock isotopes

100 mg of whole rock powder was dissolved in 4 ml of concentrated HF and 1 ml of 15 M $HNO_3$ in closed Teflon vials at 140 °C for seven days. The samples were dried down and re-dissolved in 3 ml of 15 M $HNO_3$ before being dried down again.

Sr–Nd–Pb chemical separation followed the methods described in Pin and Santos-Zalduegui (1997) and Chiaradia et al. (2011). Radiogenic isotopes of Sr, Nd and Pb were analysed at the University of Geneva using a Thermo Neptune PLUS Multi-Collector ICP-MS following the methods described by Béguelin et al. (2015) and Chiaradia et al. (2011).

Isotopic ratios were corrected for internal fractionation using $^{88}Sr/^{86}Sr = 8.375209$ for the $^{87}Sr/^{86}Sr$ ratio, $^{146}Nd/^{144}Nd = 0.7219$ for the $^{143}Nd/^{144}Nd$ ratio and $^{203}Tl/^{205}Tl = 0.418922$ for the three Pb ratios (a Tl standard was added to the solution). SRM987 ($^{87}Sr/^{86}Sr$ = 0.710248, long-term external reproducibility: 10 ppm), JNdi-1 ($^{143}Nd/^{144}Nd = 0.512115$; Tanaka et al., 2000; long-term external reproducibility: 10 ppm), and SRM 981 (Pb-isotopes; Baker et al., 2004; long-term external reproducibility of 0.0048% for $^{206}Pb/^{204}Pb$, 0.0049% for $^{207}Pb/^{204}Pb$ and 0.0062% for $^{208}Pb/^{204}Pb$) were used as external

**Table 1**
Summary of data collected from the Late Triassic rocks of the Rymill Granite Complex, Antarctic Peninsula.

| | | Samples | 18JB03 | 18JB43 | 18JB34 | 18JB18 | 18JB20 | 18JB27 | 18JB02 |
|---|---|---|---|---|---|---|---|---|---|
| | | BAS code | K7.557.1 | K7.562 | K7.526.3 | R.6306.7 | R.5786.3 | R.5290.1 | R.6067.8 |
| | | South | -68.10842 | -68.18704 | -68.20049 | -71.61314 | -70.91583 | -70.53333 | -70.69417 |
| | | West | -65.02416 | -65.30471 | -65.1823 | -66.34537 | -66.91833 | -66.8 | -66.58389 |
| | | Domain | Eastern | Eastern | Eastern | Central | Central | Central | Central |
| $^{206}Pb$-$^{238}U$ data | rims and last generation | WMA | 223±2 | 217±1 | 215±2 | 212±2 | 203±1 | 217±2 | 208±3 |
| | | MSWD | 0.86 | 1.05 | 1.12 | 1.30 | 1.00 | 1.60 | 1.06 |
| | cores | Discordia | no | no | 800±180 | 459±49 | no | no | no |
| | | MSWD | - | - | 6.7 | 0.73 | - | - | - |
| | Whole-rock isotopic tracing | $^{87}Sr/^{86}Sr_i$ | 0.708 | 0.710 | 0.709 | 0.706 | 0.707 | - | 0.714 |
| | | $^{206}Pb/^{204}Pb_i$ | 18.804 | 18.622 | 18.630 | 18.794 | 19.009 | - | 18.653 |
| | | $^{207}Pb/^{204}Pb_i$ | 15.676 | 15.672 | 15.678 | 15.674 | 15.679 | - | 15.678 |
| | | $^{208}Pb/^{204}Pb_i$ | 38.297 | 38.135 | 38.060 | 38.538 | 38.546 | - | 38.508 |
| | | $^{143}Nd/^{144}Nd_i$ | 0.512 | 0.512 | 0.512 | 0.512 | 0.512 | - | 0.512 |
| | | $\varepsilon Nd_i$ CHUR | -4.72 | -3.68 | -3.33 | -6.22 | -4.01 | - | -3.43 |
| | Whole-rock geochemistry | $SiO_2$ % | 69.70 | 65.09 | 69.37 | 70.81 | 75.14 | 63.01 | 71.18 |
| | | Th ppm | 42.14 | 32.99 | 56.21 | 18.11 | 35.52 | 6.47 | 3.90 |
| | | Nd (ppm) | 61.48 | 71.47 | 97.58 | 28.76 | 44.06 | 57.22 | 29.21 |
| | | U ppm | 3.69 | 2.50 | 5.32 | 11.30 | 5.03 | 1.70 | 0.30 |
| | | Rb (ppm) | 331.64 | 238.22 | 224.70 | 373.96 | 244.88 | 110.03 | 108.86 |
| | | Sr (ppm) | 212.71 | 349.33 | 253.47 | 135.85 | 192.99 | 1330.27 | 463.98 |
| | | $La/Yb_n$ | 28.81 | 15.03 | 32.59 | 17.40 | 13.50 | 7.10 | 12.38 |
| | | ASI | 0.97 | 1.15 | 0.98 | 1.08 | 1.03 | 0.96 | 1.04 |

standards. Due to a systematic difference between measured and accepted standard ratios, Sr, Nd and Pb isotope ratios were further corrected for external fractionation by a value of −0.039, +0.047 and +0.5 amu, respectively. Mass interferences at 84 ($^{84}Kr$), 86 ($^{86}Kr$) and 87 ($^{87}Rb$) were corrected for by monitoring $^{83}Kr$ and $^{85}Rb$. The interference of $^{144}Sm$ on $^{144}Nd$ was monitored on $^{147}Sm$ and corrected with a value of 0.206700 ($^{144}Sm/^{147}Sm$). The interference of $^{204}Hg$ on $^{204}Pb$ was corrected by monitoring $^{202}Hg$.

### 3.3. Zircon LA-ICP-MS U—Pb geochronology

The U—Pb isotopic composition of zircons was obtained using Laser Ablation Inductively Coupled Mass Spectrometry (LA-ICP-MS) at the University of Lausanne. Zircons were ablated with an UP-193FX ArF 193 nm excimer ablation system (ESI) using the following parameters: 35 μm beam size, 5 Hz repetition rate, 30 s signal and a beam energy density of 2.2–2.5 J/ cm2. Isotopic intensities were measured using an Element XR single-collector sector-field ICP-MS (Thermo Scientific). GEMOC GJ-1 zircon (CA-ID-TIMS $^{206}Pb$—$^{238}U$ age of 600.5 ± 0.4 Ma; Boekhout et al., 2012; Ulianov et al., 2012) was used as a primary standard. Secondary standards used to monitor consistency in the measured U—Pb dates were either Harvard 91500 (1065.4 ± 0.3 Ma; Wiedenbeck et al., 1995) zircon, or Plešovice (337.13 ± 0.37 Ma; Slama et al., 2008) zircon. Dates were calculated using LAMTRACE (Jackson, 2008). More details regarding the spectrometer setup and data reduction can be found in Ulianov et al. (2012). Statistical analyses of magmatic zircon data were performed using Isoplot 3.71 (Ludwig, 2003). All discordant (N1–3%) analyses of magmatic zircons were discarded. Statistical analyses of detrital zircons collected from meta-sedimentary rocks were performed using Isoplot 3.71. Only zircons with concordance >90% were accepted and plotted. All the reported results were calculated considering 2σ values.

### 3.4. Zircon in-situ Hf isotopes (LA-MC-ICP-MS)

The same zircons that were used for dating and trace element analysis were also selected for in-situ Hf isotope measurements. Analyses were carried out on a Thermo Neptune Plus MC-ICP-MS coupled to a Teledyne - Photon Machines Analyte G2 ArF excimer laser system equipped with a two volume HelEx-2 ablation cell (d'Abzac et al., 2014) at the University of Geneva. Ablation was performed at a fluence of ~4 J/ $cm^2$, a repetition rate of 5 Hz and a spot size of 40 μm (50 μm in some rare cases where enough space was available on the zircon). Helium was used as a carrier gas for the ablated particles and mixed with a small amount of $N_2$ before entering the Ar-plasma torch to increase sensitivity. Measurements were performed at low mass resolution over 120 cycles of ~1 s for standards and between 80 and 120 cycles for samples (depending on the thickness of the zircons). At the beginning of the session, the end and every ~15 sample measurements, Mud Tank, Plešovice, MUN4 and GJ-1 zircon standards were measured in order to evaluate the offset of the measured values to reference values. Blanks were also acquired (120 cycles) at the same intervals as the zircon standard measurements, but without ablation.

Data were reduced off-line using an excel spreadsheet and consisted of blank subtractions, removing the isobaric interference of $^{176}Lu$ and $^{176}Yb$ on mass 176 (e.g. Fisher et al., 2011) and correcting the resulting $^{176}Hf/^{177}Hf$ ratio for mass bias using an exponential law (Albarède et al., 2004). βHf and βYb mass bias coefficients were calculated from the measured $^{179}Hf/^{177}Hf$ and $^{173}Yb/^{171}Yb$ with the reference values of Patchett and Tatsumoto (1981) ($^{179}Hf/^{177}Hf = 0.7325$) and Thirlwall and Anczkiewicz (2004) ($^{173}Yb/^{171}Yb = 1.1234$) respectively. Isobaric interferences of $^{176}Yb$ and $^{176}Lu$ with $^{176}Hf$ were corrected using $^{176}Yb/^{173}Yb = 0.786954$ and $^{176}Lu/^{175}Lu = 0.02645$ respectively (Thirlwall and Anczkiewicz, 2004). Only non-perturbed spectra were retained. Initial $^{176}Hf/^{177}Hf$ ratios and initial εHf were calculated using the $^{206}Pb/^{238}U$ date of the respective crystal, the CHUR parameters of Bouvier et al. (2008) ($^{176}Hf/^{177}Hf = 0.282785$ and $^{176}Lu/^{177}Hf = 0.0336$) and $\lambda^{176}Lu = 1.87 \times 10–11$ year-1 (Söderlund et al., 2004).

As no Temora standard was available for measurement but its $^{173}Yb/^{177}Hf$ values are closer to our zircon samples than the $^{173}Yb/^{177}Hf$ values of the other standards measured, the long term in-house standard deviation on the age corrected εHf from the Temora standard as well as its offset value of the age corrected εHf from its nominal value were used (e.g. Rezeau et al., 2016) to calculate the standard deviation (*2std propagated including offset*) on the age corrected εHf values from the samples. The standard deviations of the Temora standard zircon (Rezeau et al., 2016) are higher than those obtained during the analytical sessions of the present work on the Mud Tank, Plešovice and GJ-1 zircon standards. Additionally, the standard deviations associated with the measurements of Mud Tank, Plešovice and GJ-1 obtained during our analyses were lower than the long-term inhouse standard deviations obtained by Rezeau et al. (2016), which gives us confidence

on the reproducibility of our data at least at the same level as that obtained by Rezeau et al. (2016). This conservative approach was chosen in order to make sure that we did not underestimate the standard deviations applied to our final results; on the contrary, it most likely slightly overestimates the uncertainties.

### 3.5. O isotopes in zircon

Oxygen isotopes ($^{18}O$, $^{16}O$) in zircon were analysed using a Cameca IMS 1280-HR multicollector ion microprobe at the Institute of Earth Sciences of the University of Lausanne (Switzerland). A 133Cs + primary beam with impact energy of 10 kV and beam current of ~ 2.0 nA with a ~10 μm spot size was used. The electron flood gun, with normal incidence, was used to compensate charges. $^{16}O$ and $^{18}O$ secondary ions, accelerated at 10 kV, were analysed with a mass resolving power of 2400 and the ion signals were collected on faraday cups in multi-collection mode. Mass calibration was performed at the beginning of the session, which lasted 16 h. A single analysis took 4 min, including pre-analysis rastering, automated secondary ion tuning, and 90 s of continuous peak counting. Instrumental mass fractionation and detector gain were monitored by repeated analysis of Temora-2 zircon as primary standard ($\delta^{18}O_{VSMOW}$ = 8.20‰; Black et al., 2004) with four analysis of the reference material taken after every 13 unknowns. An average reproducibility of 0.28‰ (2SD) on the Temora-2 zircon reference material was observed for the whole session, and internal error for each analysis was lower than 0.3‰ (2SE). Mud Tank zircon grains were used as reference material (Valley, 2005) and measured 7 times during the session. A reproducibility of 0.49‰ (2SD) was observed for Mud Tank zircon grains. Oxygen isotopic analyses of Mud Tank normalised to Temora 2 yielded an average measured value of 4.93‰, comparable to the published value of 5.03‰ (Valley, 2005). All oxygen isotope values reported here are in per mil (‰) and relative to VSMOW (Vienna Standard Mean Ocean Water). The zircon oxygen isotope data are presented in Bastias et al. (2019b).

## 4. Results

### 4.1. Rock samples

Seven orthogneisses, with abundant hornblende, white mica and biotite were collected from the crystalline basement of the Antarctic Peninsula and provided by the British Antarctic Survey (BAS). Three of these are located in the Eastern Domain, and four are from the Central Domain using the nomenclature of Vaughan and Storey (2000). Petrographic analysis reveals intense irregular, migrated and bulged boundaries between crystals, revealing dynamic recrystallization that appears more intense in both feldspars and quartz.

### 4.2. Zircon U—Pb geochronology and Hf—O isotope geochemistry

#### 4.2.1. Eastern domain

Three hornblende and micaceous orthogneisses were analysed from the Eastern Domain, in the region of southern Graham Land (Fig. 2). Cathodoluminescence analyses of zircons (Fig. 3) revealed two groups of textures present in all the samples: i) oscillatory zonation with distinct cores, and ii) patchy and homogenous zoning, with an absence of rim-core relationship, typically founded in igneous rocks (e.g. Chelle-Michou et al., 2014). Both the rims of the zoned zircons, and the unzoned zircons yield indistinguishable dates from any given rock, which, when combined with the style of cathodoluminescence zonation, supports an igneous origin. However, we acknowledge that without trace element compositions of the zircons, there is some ambiguity as to the origin of the youngest generation of zircons in these rocks. Ablation of zircon rims from orthogneiss 18JB34 yields five $^{206}Pb/^{238}U$ concordia ages that span between 217 ± 2 Ma and 212 ± 2 Ma, and yield a weighted mean $^{206}Pb/^{238}U$ age of 215 ± 1 Ma (MSWD = 1.1; Figs. 3 and 4a, Table 1). Inherited cores mostly yield discordant U—Pb dates, while some weakly define a discordia with an imprecise upper intercept age of 800 ± 180 Ma (MSWD = 6.7; Fig. 4a), suggesting entrainment of Neoproterozoic crustal material. The Hf isotopic compositions of the zircon rims yield $\varepsilon Hf_t$ values that range from −5.5 to −2.9 (Fig. 5a), corresponding to Lu—Hf model ages ($TDM_{Hf}$) between 1.20 and 1.05 Ga. Finally, the Late Triassic zircons yield $\delta^{18}O$ values that range between 8.1 and 7.5% (Fig. 6b). Analyses of the rims of zircons extracted from orthogneiss 18JB43 yield nine $^{206}Pb/^{238}U$ concordia ages spanning between 219 ± 2 Ma and 216 ± 2 Ma, with a weighted mean $^{206}Pb/^{238}U$ age of 217 ± 1 Ma (MSWD = 1.05; Figs. 3 and 4b, Table 1). Inherited cores yielded concordant ages of 1055 ± 8 Ma (Fig. 4b). Hf isotopic compositions of the rims of the same zircons that were dated yield $\varepsilon Hf_t$ values that range from −5.1 to −3.2 (Fig. 5b), corresponding to Lu—Hf model ages between 1.18 and 1.08 Ga. $\delta^{18}O$ values collected from the Late Triassic zircon rims range between 8.1 and 7.3% (Fig. 6b). Finally, ablation of the rims of zircons extracted from orthogneiss 18JB03 yields twelve $^{206}Pb/^{238}U$ concordia ages that span between 225 ± 5 Ma and 218 ± 7 Ma, with a weighted mean $^{206}Pb/^{238}U$ age of 223 ± 2 Ma (MSWD = 0.86; Figs. 3 and 4c, Table 1). The Triassic zones of the zircons yielded Lu—Hf model ages between 1.29 and 1.06 Ga. Some ablation spots on the zircon cores gave $^{206}Pb/^{238}U$ concordia ages of 259 ± 5, 580 ± 13 Ma, 605 ± 7 and 966 ± 21 Ma (Fig. 4c). Late Triassic rims give $\varepsilon Hf_t$ values that range from −6.5 to −2.8, while the inherited zircon cores yield $\varepsilon Hf_t$ values between 2.7 and − 2.6 (late Neoproterozoic), and 10.8 and 5.8 (early Neoproterozoic). The Lu—Hf model ages in the inherited cores of the zircons yield values between 1.33 and 0.90 Ga, while the Late Triassic rims yield model ages of 1.26 and 1.06 Ga. A comparison of the $^{206}Pb/^{238}U$ ages of the zircon rims and cores with their $\varepsilon Hf_t$ values reveals a general positive trend, albeit with significant time gaps (Fig. 5c). Triassic zircon rims yield $\delta^{18}O$ values between 9.6 and 7.0% (Fig. 6b).

Summarising, three orthogneiss samples from the Eastern Domain yield weighted mean $^{206}Pb/^{238}U$ ages from zircon rims that span between 223 and 215 Ma, which yield no clear trends when compared with their $\varepsilon Hf_t$ and $\delta^{18}O$ values (Figs. 6a, b). Inherited zircon cores yield $^{206}Pb/^{238}U$ concordia ages that range from the late Cambrian to the Neoproterozoic and late Mesoproterozoic (Fig. 7). The quantity of Hf isotopic data collected from xenocrystic zircon cores is insufficient to identify any robust trends (7 analyses spanning ~700 Ma; Fig. 6c). Regardless, Hf isotopic data from Precambrian cores reveals more radiogenic sources compared to the Triassic rims, although the Lu—Hf model ages of all age groups fall within the same range (1.33–0.90 Ga; Fig. 6c).

#### 4.2.2. Central Domain

Four hornblende bearingmicaceous orthogneisses have been analysed from the Central Domain, which have been sampled from northwestern Palmer Land to the east of Alexander Island (Fig. 2). Cathodoluminescence analyses of the zircons revealed similar characteristics to the Eastern Domain (Fig. 3), showing characteristic igneous patchy zonation, and distinct cores and rims in all four orthogneisses.

Analysis of the rims of zircons from orthogneiss 18JB20 yield nine $^{206}Pb/^{238}U$ concordia ages that range between 205 ± 2 Ma and 202 ± 3, with a weighted mean $^{206}Pb/^{238}U$ age of 203 ± 1 Ma (MSWD = 1.00; Fig. 3; Table 1). All analyses of the cores yielded discordant dates with no clear discordia (Fig. 4d). The Hf isotopic compositions of the Triassic zircon rims yield $\varepsilon Hf_t$ values that range from −5.1 to −2.8 (Fig. 5d), with no clear trend with time, and correspond to Lu—Hf model ages between 1.16 and 1.04 Ga. $\delta^{18}O$ values obtained from Late Triassic zircons range between 6.9 and 5.8%, which are distinguishably lower than all other rocks from both domains, and approach mantle compositions (Fig. 6b; 5.3 ± 0.6%, Valley et al., 2005). Ablation of the rims of zircons from orthogneiss 18JB02 gives five $^{206}Pb/^{238}U$ concordia ages that range between 212 ± 7 Ma and 204 ± 6 Ma, with a weighted

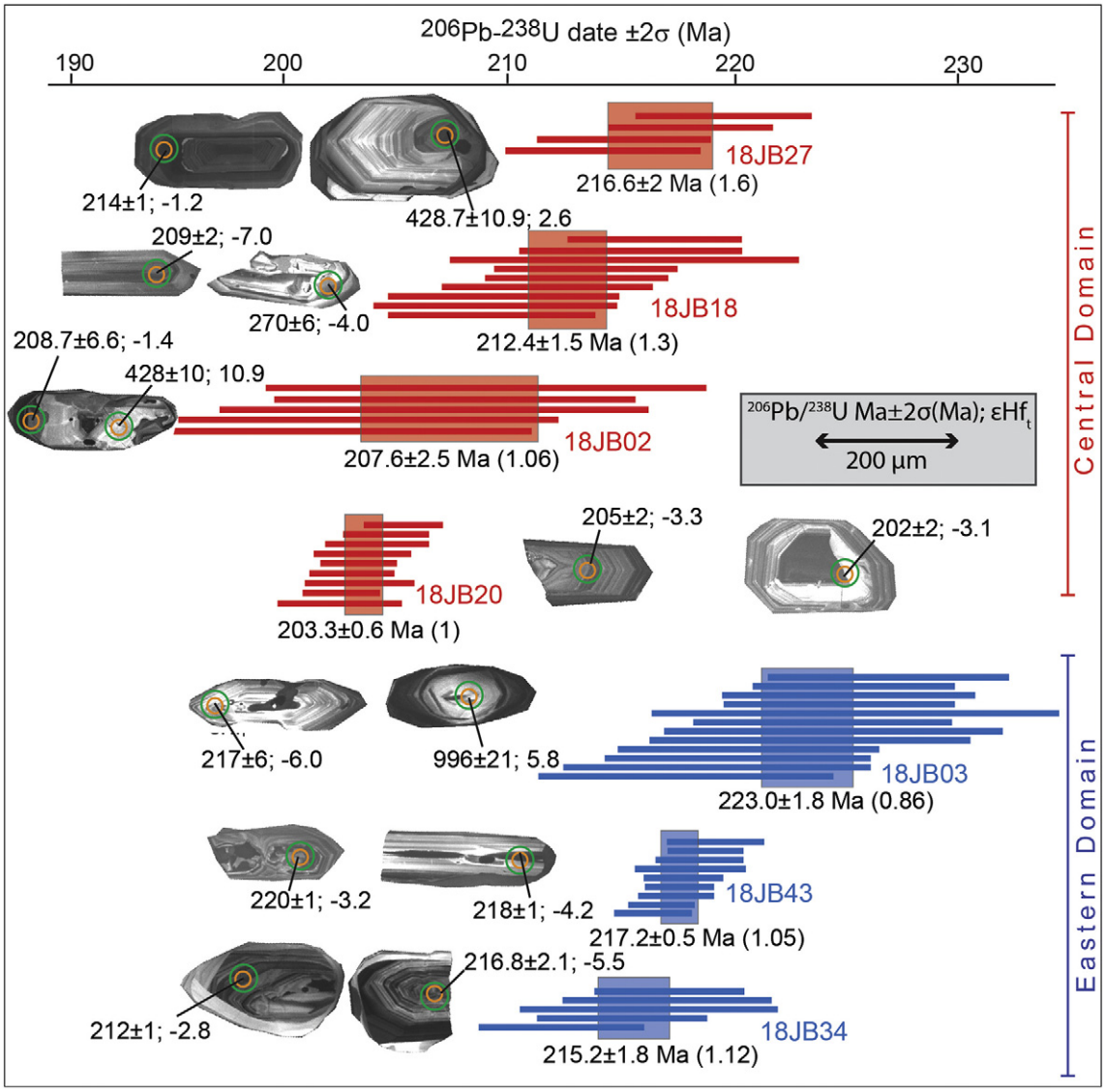


**Fig. 3.** Selected zircon $^{206}U$–$^{238}Pb$ concordia ages and $\varepsilon Hf_t$ values obtained from orthogneisses in the Eastern (data in blue) and Central (data in red) domains of the Antarctic Peninsula. Bars represent single ablation spots and represent an uncertainty of 2σ. Weighted mean ages are shown along with the associated MSWD (in brackets). Representative cathodoluminescence (SEM) images of the dated zircons are presented, and reveal oscillatory zoning, and xenocrystic cores with magmatic rims. Ablation spot locations are shown (green Hf; orange U–Pb).

mean $^{206}Pb/^{238}U$ age of 208 ± 5 Ma (MSWD = 1.06; Figs. 3 and 4e, Table 1). Zircon cores yield concordant Permian – Ordovician ages, ranging between 266 ± 3 Ma and 466 ± 5 Ma (Fig. 4e). Late Triassic zircon rims have initial $\varepsilon Hf_t$ values that range from −1.8 to −1.0, while the inherited zircon cores yield $\varepsilon Hf_t$ values ranging between 2.6 and −4.6 (Fig. 5e), corresponding to Lu—Hf model ages between 0.99 and 0.94 Ga and between 1.24 and 0.89 Ga, respectively. These data do not define a clear trend of Hf compositions with crystallisation age (Fig. 5e). Late Triassic zircon rims yield $\delta^{18}O$ values that range between 9.9 and 7.4‰.

Analyses of the rims of zircons from orthogneiss 18JB18 yield nine $^{206}Pb/^{238}U$ concordia ages that range between 214 ± 4 Ma and 209 ± 2 Ma, with a weighted mean $^{206}Pb/^{238}U$ age of 212 ± 2 Ma (MSWD = 1.3; Figs. 3 and 4f; Table 1). A single inherited core yielded a $^{206}Pb/^{238}U$ concordia age of 271 ± 3 Ma (Permian). Some inherited cores yield discordant U—Pb dates, and define a discordia with an upper intercept age of 459 ± 49 Ma (MSWD = 0.73; Fig. 4f). Hf isotopic compositions of the Late Triassic rims that yield concordant U—Pb dates have $\varepsilon Hf_t$ values that range from −8.8 to −5.0 (Fig. 5f), corresponding to Lu—Hf model ages between 1.38 and 1.17 Ga. $\delta^{18}O$ values collected from Late Triassic zircons yield values between 9.1 and 7.6‰. A $\varepsilon Hf_t$ value of −4.1 was collected in a zircon core with a $^{206}Pb/^{238}U$ concordia age of 271 ± 3 Ma, which yields a $TDM_{Hf}$ of 1.17 Ga. Finally, orthogneiss 18JB27 only yielded four $^{206}Pb/^{238}U$ concordia ages from zircon rims that range between 214 ± 2 Ma and 219 ± 2 Ma, with a weighted mean $^{206}Pb/^{238}U$ age of 217 ± 2 Ma (MSWD = 1.6; Figs. 3a and 4g, Table 1). Analysis of zircon cores yielded $^{206}Pb/^{238}U$ concordia ages that are Permian (253 ± 2 to 295 ± 3 Ma), Carboniferous (312 ± 7 to 358 ± 6 Ma), Devonian (393 ± 4 and 403 ± 4 Ma), Silurian (424 ± 4 to 441 ± 4 Ma), Ordovician (448 ± 4 to 487 ± 5 Ma), Cambrian (502 ± 4 and 528 ± 6 Ma) and Neoproterozoic (751 ± 6 and 770 ± 8 Ma; Fig. 4g). Hf isotopic compositions in the Late Triassic zircon rims yield $\varepsilon Hf_t$ values between −5.1 and −1.2, corresponding to $TDM_{Hf}$ ages spanning between 1.18 and 0.97. Inherited cores yielded $\varepsilon Hf_t$ values between 10.8 and −8.3 with Lu—Hf model ages spanning between 1.37 and 0.73 Ga. The Hf data define a trend towards less radiogenic Hf compositions with younger crystallisation ages during the Palaeozoic (Fig. 5g).

Summarising, zircon rims extracted from orthogneisses in the Central Domain yield concordant, Late Triassic $^{206}Pb/^{238}U$ ages ranging

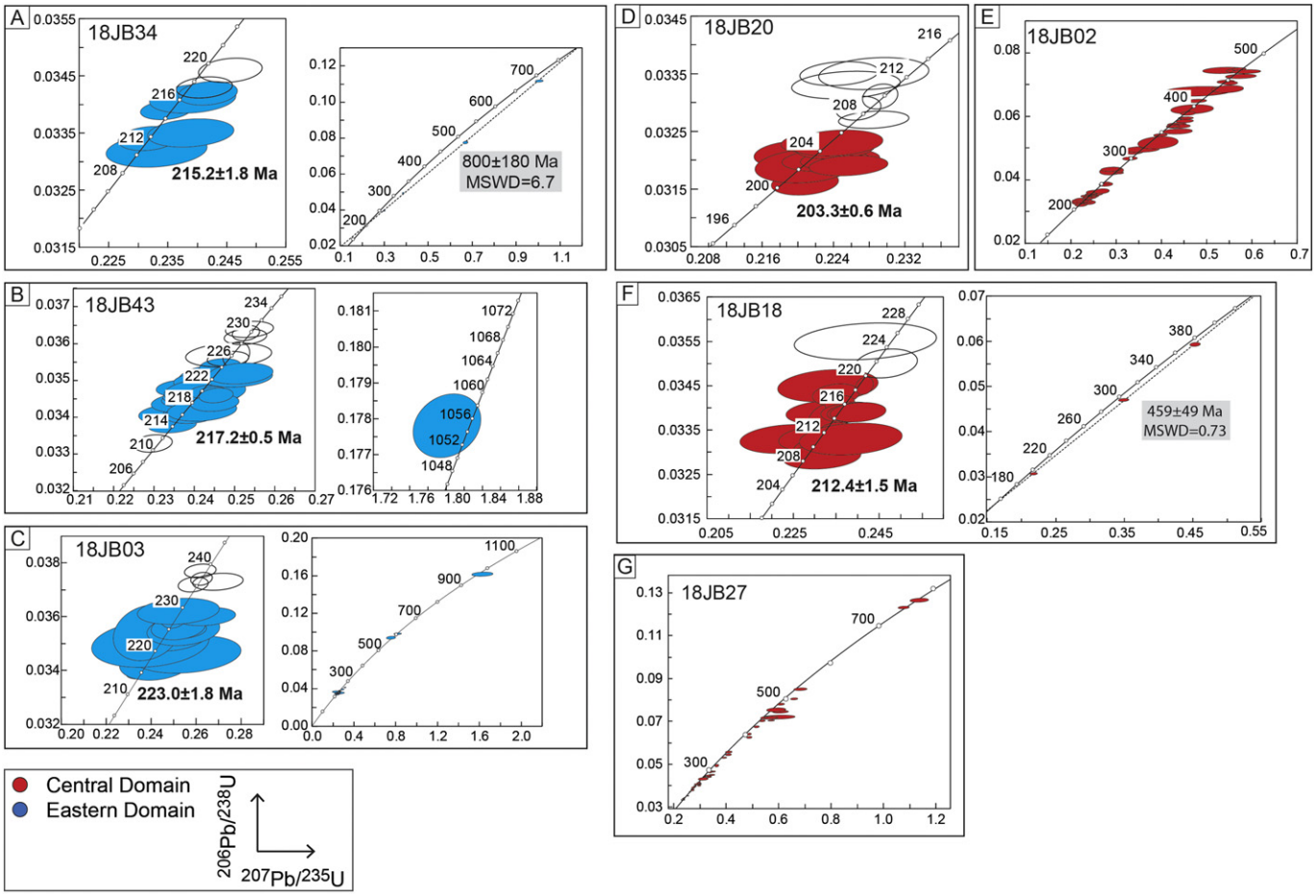


**Fig. 4.** Representative Wetherill concordia plots of zircon U—Pb data obtained from Triassic orthogneisses of the Antarctic Peninsula. Coloured ellipses are included in the weighted mean age calculations. Discordia and xenocrystic ages are shown in some cases.

between 217 ± 2 and 203 ± 1 Ma, with $\varepsilon Hf_t$ values ranging between −8.8 and −1.0 (Fig. 6a, Table 1). The same zircon rims yielded $\delta^{18}O$ values that span between 9.9 and 5.8% (Fig. 6b), suggesting they formed by melting heterogeneous crustal sources with variable amounts of mantle input, corroborating the Hf isotopic compositions. These ages are generally younger than those in the Eastern Domain, although the age ranges overlap (Fig. 3 and 6a). Inherited zircon cores have concordant $^{206}Pb/^{238}U$ ages that generally span the Palaeozoic, with few Neoproterozoic ages (Fig. 7). In contrast, there is a paucity of Palaeozoic cores in the Eastern Domain (Fig. 7 and 6b). The $\varepsilon Hf_t$ values for Devonian to Silurian zircon cores show a tendency towards more depleted Hf isotopic compositions with younger ages, although these are consistent with common Lu—Hf model ages for the same time period (Fig. 6c).

### 4.3. Whole rock geochemistry and Sr–Nd–Pb isotopic compositions

#### 4.3.1. Whole rock major oxides and trace elements

Whole rock major oxides, trace elements and Rare Earth Elements (REE) have been obtained from the same orthogneisses that yield Late Triassic $^{206}Pb/^{238}U$ ages from zircon rims. A majority of the rocks are classified as alkali granites in the cationic scheme of De La Roche et al. (1980) (Fig. 8a), although a single syenogranite and quartz syenite were also sampled. $SiO_2$ values span between 75.1 and 63.0 wt% in the Central Domain and between 69.7 and 65.0% in the Eastern Domain (Fig. 8b, c and d; Table 1). All orthogneisses plot close to the ferroan-magnesian boundary of Frost et al. (2001) with a tendency to magnesian values (Fig. 8b). The orthogneisses span between the calc-alkaline and alkali-calcic differentiation trends on the modified alkali-lime index of Frost et al. (2001) (Fig. 8c), and high-K calc-alkaline to shoshonitic fields when comparing $SiO_2$ with $K_2O$ (Fig. 8d). The Triassic rocks yield Aluminum Saturation Indices (Maniar and Piccoli, 1989) that range between 0.96 and 1.08 in the Central Domain, and 0.97 to 1.15 in the Eastern Domain (Fig. 8e), and thus lie proximal to the metaluminous-peraluminous boundary. A comparison of $K_2O$ and $Na_2O$ shows the orthogneisses span the I- and S-type fields of Chappell and White (1974) (Fig. 8f). Tectonic discrimination diagrams using (Y + Nb) and Rb from Pearce et al. (1984) suggests these Triassic rocks formed within a *syn*-collisional, arc or within plate setting (Fig. 8g). N-MORB normalised REE abundances in the Late Triassic orthogneisses reveal light-REE (LREE) enrichment (Fig. 8h) relative to heavy-REE (HREE), with $(La/Yb)_N$ ranging between 7.1 and 17.4 in the Central Domain and between 15.0 and 32.5 in the Eastern Domain (Table 1). N-MORB normalised trace element abundances (values from Sun and McDonough, 1989; Fig. 8i) show that Late Triassic rocks of the Eastern and Central domains are extremely similar, suggesting there are no distinct changes in fractionation assemblages or assimilation between these domains. Trace elements in all orthogneisses are enriched in Light Ion Lithophile Elements (LILE), and negative Nb, Ta, Sr and Ti anomalies suggests that a subduction derived component is incorporated into these rocks, and it is likely that they formed within a continental arc. These Triassic rocks yield minor negative Ba, Eu and Sr anomalies, combined with a strong negative Ti anomaly, which suggests that plagioclase and Fe—Ti oxides have fractionated, and the positive Pb anomaly is likely to have been derived from an upper crustal source. Trace element concentrations of the Triassic rocks normalised to average upper continental crust (Taylor and McLennan, 1995; Fig. 8j) scatter close to unity, supporting a crustal origin for these orthogneisses. A

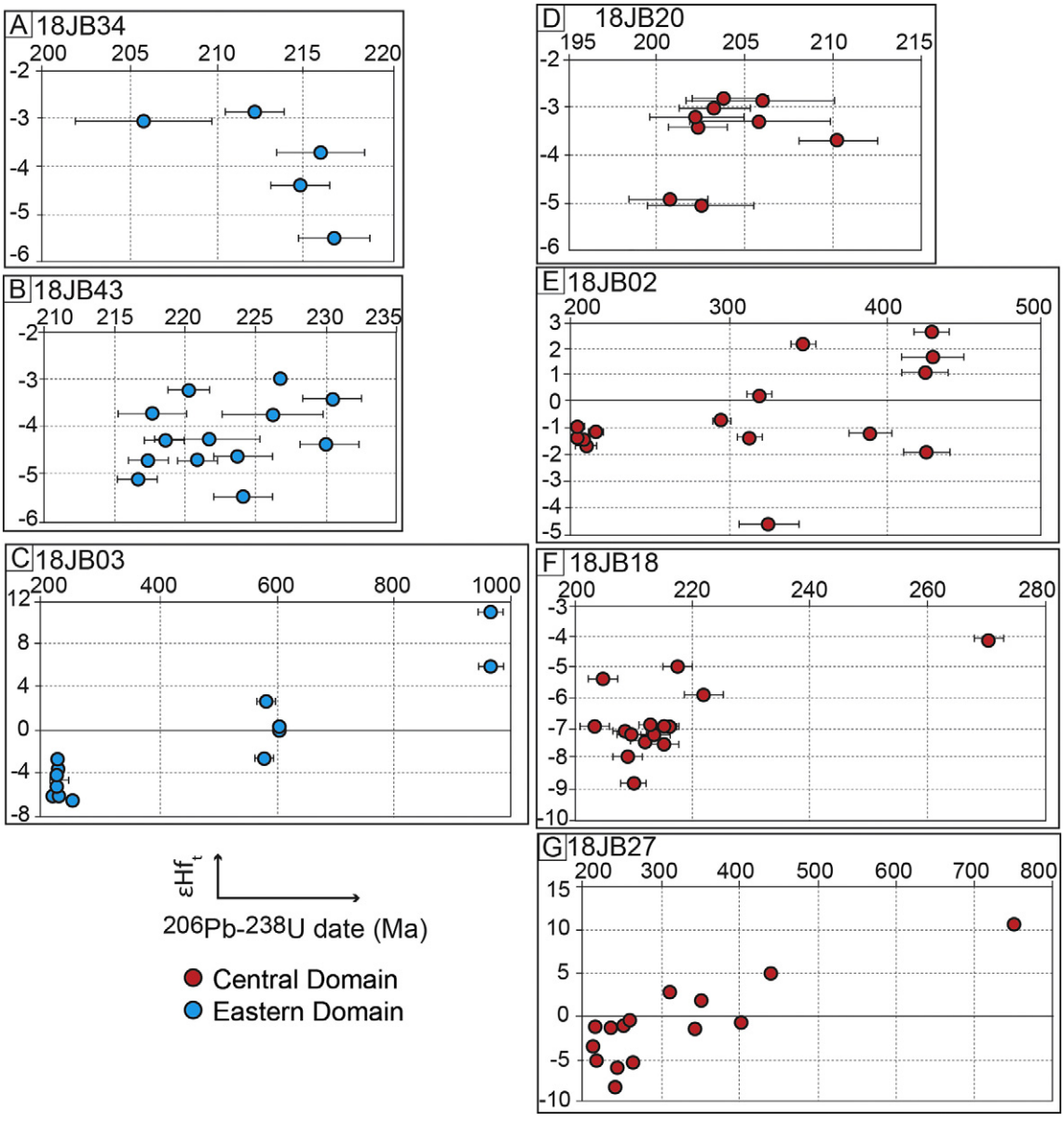


**Fig. 5.** A comparison of $^{206}$Pb—$^{238}$U zircon concordia ages and zircon εHf$_t$ for grains analysed in this study. 2σ uncertainties are ~ ± 5% for U—Pb zircon ages (full dataset in Bastias et al., 2019b).

comparison of chondrite normalised La/Yb with the Triassic crystallisation ages (Fig. 8k) yields no particular trend.

*4.3.2. Whole rock (Sr-Nd-Pb) isotopic compositions*

The Late Triassic orthogneisses with ages ranging between 223.0 ± 1.8 and 203.3 ± 0.6 Ma yield time corrected whole rock ($^{87}$Sr/$^{86}$Sr)$_i$ values that range between 0.7096 and 0.7076 (Table 1, Fig. 9a) in the Central Domain, and 0.7140 and 0.7061 in the Eastern Domain (Table 1, Fig. 9a), which are more radiogenic than present-day depleted mantle ($^{87}$Sr/$^{86}$Sr ~0.702; Zindler and Hart, 1986). Whole rock εNd$_i$ values are less radiogenic than CHUR (e.g. Bouvier et al., 2008), and range between −6.22 and −3.43 in the Central Domain and −4.7 and −3.3 in the Eastern Domain (Fig. 9a). Neither the whole rock ($^{87}$Sr/$^{86}$Sr)$_i$ nor the εNd$_i$ show any trends when compared with crystallisation age. The εHf$_t$ values for all Triassic zircon rims from the Eastern and Central Domain are indistinguishable, vary between −8.8 and − 1.0 and thus are less radiogenic than CHUR (Bouvier et al., 2008), and show no trends with crystallisation age (Fig. 8a).

Whole rock Pb isotopic compositions of the Triassic orthogneisses (Table 1) range between 19.00 and 18.65 ($^{206}$Pb/$^{204}$Pb$_i$), 15.679–15.673 ($^{207}$Pb/$^{204}$Pb$_i$) and 38.54–38.50 ($^{208}$Pb/$^{204}$Pb$_i$) in the Central Domain, and 18.80–18.62 ($^{206}$Pb/$^{204}$Pb$_i$), 15.678–15.671 ($^{207}$Pb/$^{204}$Pb$_i$), and 38.29–38.06 ($^{208}$Pb/$^{204}$Pb$_i$) in the Eastern Domain, revealing no distinguishable variations between these regions (Fig. 9b). These Pb isotope compositions support an enriched mantle source mixed with upper continental crust and/or continent derived sediments (Fig. 9b). Finally, all the orthogneisses yielded εNd$_i$ values that correlate well with zircon εHf$_t$ (Fig. 9c), and they plot between the trends defined by global recycled orogenic sands and the global mantle array (Vervoort et al., 1999).

## 5. Interpretation

*5.1. Late Triassic anatexis and magmatic sources*

New concordant $^{206}$Pb/$^{238}$U dates from the rims of zircons reveal a series of metamorphosed alkali granites, syenogranites and quartz-

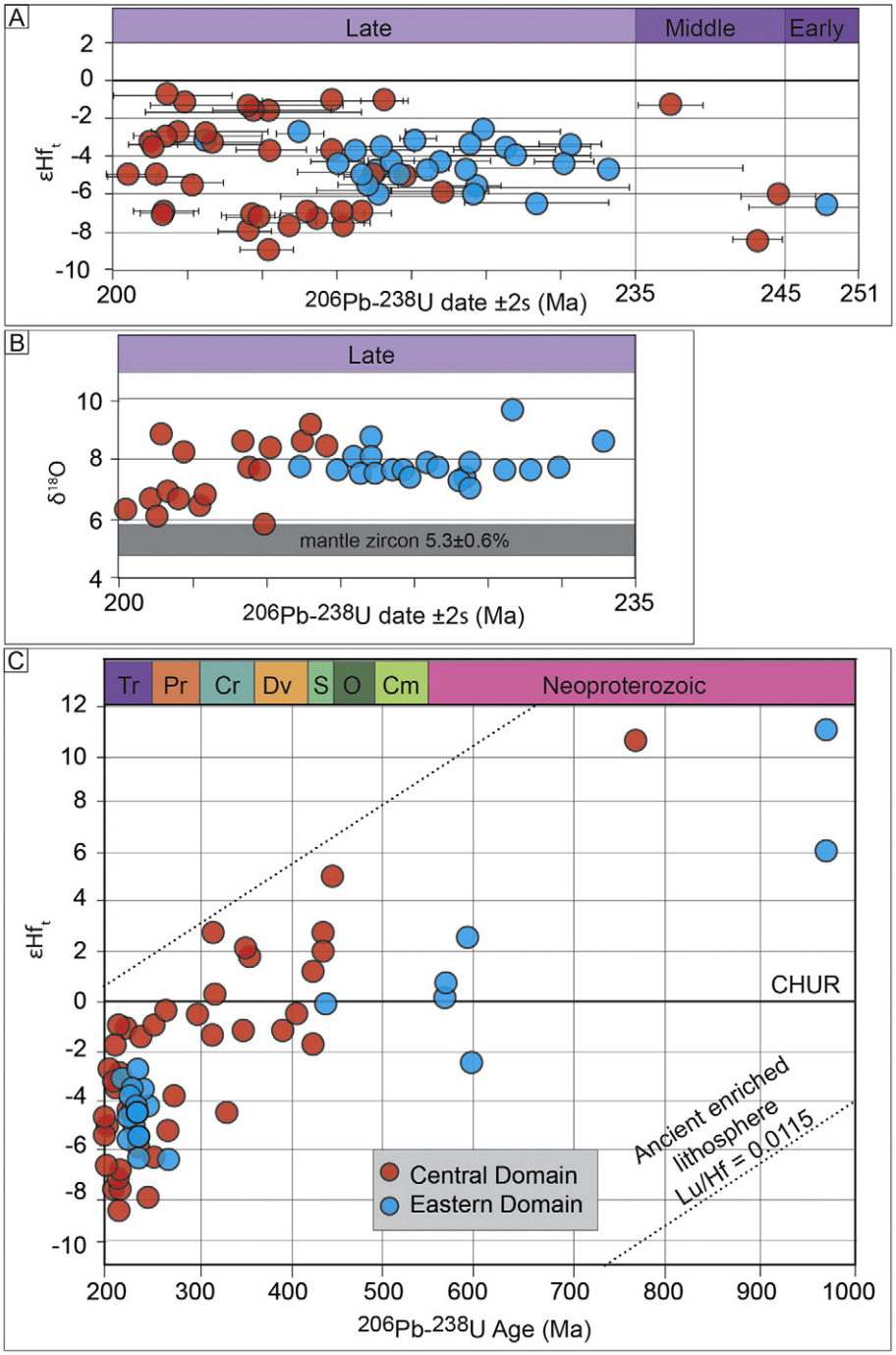


**Fig. 6.** A comparison of $^{206}Pb—^{238}U$ concordia ages and $\varepsilon Hf_t$ (A) and $\delta^{18}O$ (B) from zircon rims within Triassic orthogneisses of the Antarctica Peninsula. The mantle zircon $\delta^{18}O$ value is from Valley et al. (2005). (C) A comparison of $^{206}Pb—^{238}U$ concordia ages and $\varepsilon Hf_t$ from inherited zircon cores and rims within the Triassic orthogneisses. 2σ uncertainties are ~ ± 7% for U—Pb zircon ages (full dataset in Bastias et al., 2019b) and 4% for the $\delta^{18}O$ values.

syenites that crystallised between 223 ± 2 and 203 ± 1 Ma, and are dispersed throughout the Central and Eastern domains of the Antarctic Peninsula, as defined by Vaughan and Storey (2000) (Fig. 1). This range is consistent with previously reported (Millar et al., 2002; Flowerdew et al., 2006) zircon U—Pb dates from similar lithologies that span between 236 ± 2 and 206 ± 4 Ma (Fig. 2). Collectively, all of these outcrops are dispersed over a distance of ~250 km, and thus they are considered to be of regional significance within the Antarctic Peninsula. The crystallisation ages of zircons in the Eastern Domain span between 237 ± 2 and 215 ± 2 Ma, which overlap with but are older than those from the Central Domain, which range between 228 ± 6 and 203 ± 1 Ma (Fig. 2). We now informally refer to these gneissic Triassic intrusions as the Rymill Granite Complex, to differentiate them from the less foliated and more geographically widespread Jurassic intrusions.

The dated rocks are predominantly calc-alkaline orthogneisses that plot along the metaluminous-peraluminous boundary of Maniar and Piccoli (1989), yield $Na_2O/K_2O$ ratios that range between 0.50 and 1.17, and yield upper continental crust normalised multi-element abundances that are close to unity. Trace element concentrations reveal the substantial presence of a subduction derived component in their source, and it is likely that these rocks formed within a continental arc setting.

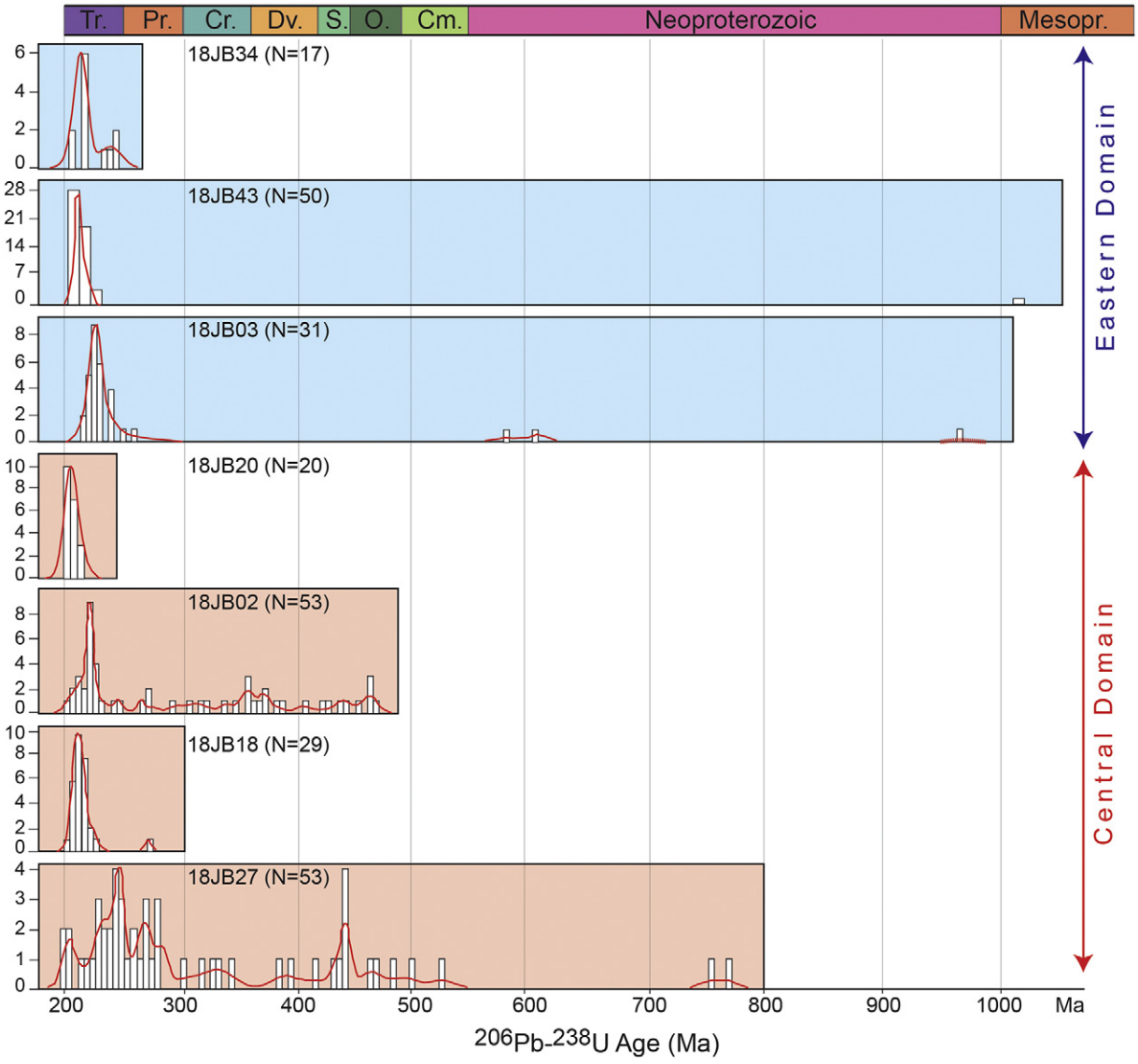


**Fig. 7.** Histogram and Kernel Density Estimates (red line) of zircon $^{206}Pb$—$^{238}U$ concordia ages obtained from the Late Triassic orthogneisses of the Antarctic Peninsula.

The Triassic orthogneisses from the Eastern and Central domains yield indistinguishable major oxide, REE and trace element concentrations, and it is likely that they evolved via the same magmatic processes.

The Hf and O (rims and youngest generation of zircons), and Sr, Nd and Pb (whole rock) isotopic compositions from the Late Triassic orthogneisses in both the Eastern and Central domains are similar, and no distinct trends are identified in $\varepsilon Hf_t$ (−8.8 to 1.0), $\delta^{18}O$ (9.6 to 5.7), $\varepsilon Nd_t$ (−6.22 to −3.33) and $^{87}Sr/^{86}Sr_i$ (0.7061–0.7140) with time (Fig. 6 and 9a). These data suggest that the Triassic orthogneisses in both domains formed by melting similar source rocks. Furthermore, these isotopic compositions do not reveal any direct input from depleted mantle sources (e.g. $\delta^{18}O > 6.5\%$ can equate to a sedimentary source; Valley et al., 1998; Kemp et al., 2006), which is consistent with the high $SiO_2$ contents, and the major oxide and trace element compositions of the rocks. The values and large range in the Hf—O (zircon), Sr and Nd (whole rock) isotopic compositions supports a derivation from mixed sources that resided within the continental crust.

Previous interpretations of geochemical and isotopic data obtained from the Triassic orthogneisses assigned an S-type affinity (Wever et al., 1994; Scarrow et al., 1996; Leat et al., 1995). However, we find that the Triassic orthogneisses are difficult to classify using the I- and S-type scheme and their major element compositions. The metaluminous-peraluminous character combined with $Na_2O/K_2O$ ratios that straddle the I- and S-type fields of Chappell and White (1974) suggests that both I- and S- type granites have formed coevally. For example, biotite and white mica bearing orthogneiss 18JB18 (214.4 ± 1.5 Ma) yields an ASI of 1.08 and has whole rock $\varepsilon Nd_t$ (−6.2) values that resemble S-type characteristics (Chappell and White, 1974). In contrast, hornblende bearing orthogneiss 18JB34 (215.2 ± 1.8 Ma) has an ASI of 0.98, and a whole rock $\varepsilon Nd_t$ value of −3.9, which are closer to I-type characteristics. These data suggest that the Late Triassic magmas formed by melting both sedimentary and igneous crustal sources, which mixed to various degrees, forming the large scatter in time-corrected isotopic compositions, and geochemical compositions that straddle I- and S-type criteria (e.g. Chappell and White, 1974, 1992; Clemens, 2003; Clemens et al., 2011; Gao et al., 2016).

A comparison of the zircon $\varepsilon Hf_t$ and whole rock $\varepsilon Nd_t$ isotopic systems reveals a reasonable correlation (Fig. 9c), and orthogneisses from both the Eastern and Central domains plot between the trends defined by global recycled orogenic sands and the global mantle array (Vervoort and Patchett, 1996; Vervoort et al., 1999). This correlation suggest that garnet fractionation was not an important process in the

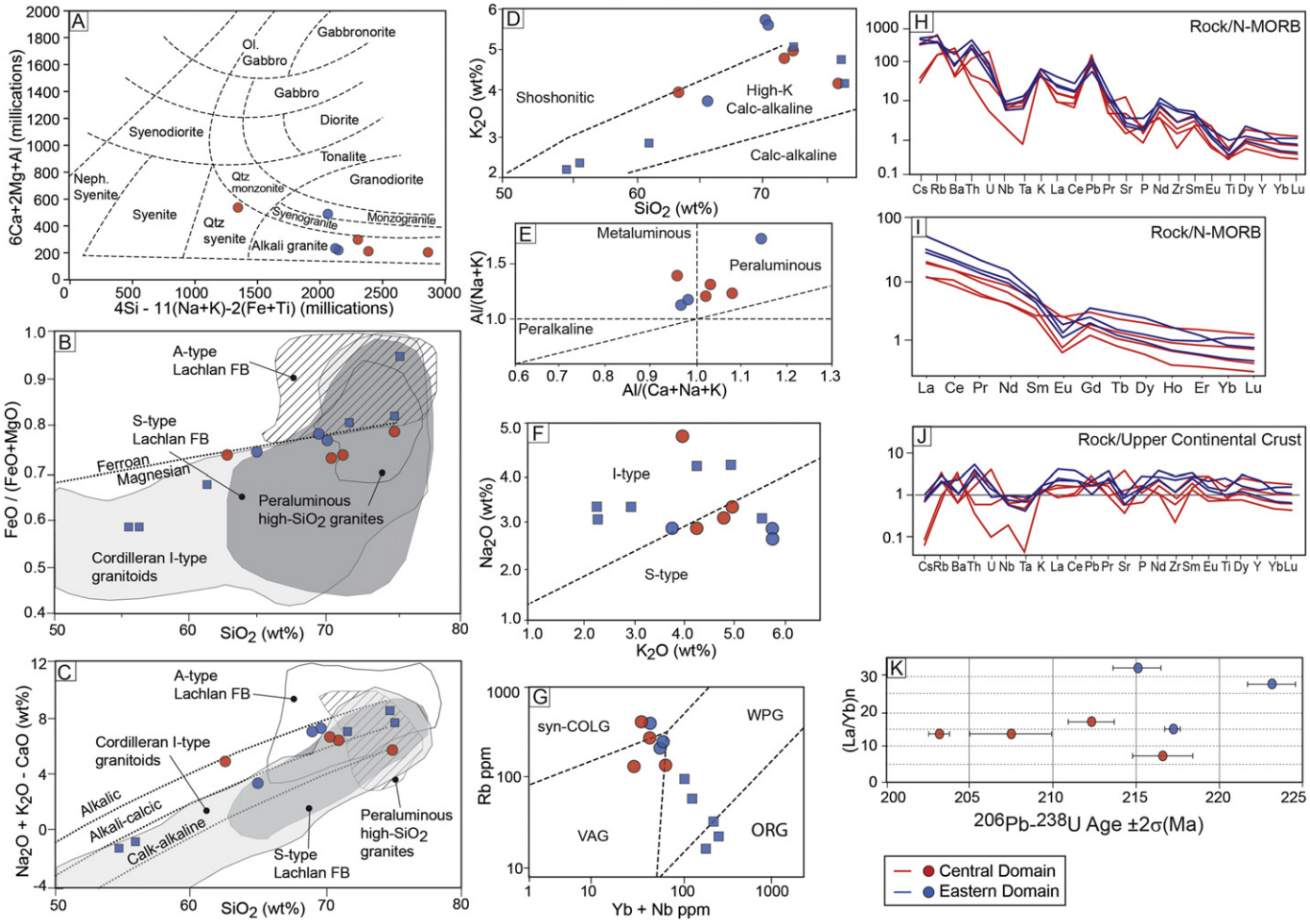


**Fig. 8.** Geochemical data from Triassic orthogneisses from the Eastern and Central domains of the Antarctic Peninsula. (A) Multi-cation discrimination plot from De La Roche et al. (1980), (B) FeO number vs. wt% $SiO_2$, showing the boundary between ferroan and magnesian plutons, and regions for Mesozoic Cordilleran I-type, A- and S-type as defined by rocks in the Lachlan Fold Belt (Frost et al., 2001; Landenberg and Collins. 1996). (C, D) Modified alkali-lime index of Peacock (1931) showing the ranges for the alkalic, alkali calcic, calc-alkaline, and calcic rock series. For any given suite, the $SiO_2$ value where the modified $Na_2O + K_2O - CaO$ index (MALI) equals 0 corresponds to the original alkali-lime index of Peacock. (E) Aluminum saturation index (ASI) plot of Maniar and Piccoli (1989), (Al/Na + K) and (Al/Ca + Na + K) are defined as molecular ratios and take into account the presence of apatite so that rocks with ASI > 1.0 are corundum normative and are termed peraluminous (Zen, 1988). (F) $Na_2O$ vs $K_2O$ diagram with the fields of I- and S-type rocks from Chappell and White (1974). (G) Rb vs Yb + Nb discrimination diagram for tectonic settings from Pearce et al. (1984), blue squares are from Scarrow et al. (1996). WPG: within plate granites, VAG: volcanic arc granites, ORG: ocean ridge granites, *syn*-COLG: syn-collisional granites, post-COLG: post-collisional granites. (H, I) Rare earth element and trace element abundances normalised to N-MORB values of Sun and McDonough (1989). (J) Trace elements abundances normalised to Upper Continental Crust (Taylor and McLennan, 1995). (K) N-MORB normalised La/Yb vs the Triassic crystalisation ages of the zircon rims.

melt source region, and thus the Lu—Hf model ages may approximate the average age of extraction of the various components of the melt source from the depleted mantle (e.g. Hawkesworth and Kemp, 2006). Regardless of whether the source regions for the Late Triassic rocks contained igneous or sedimentary protoliths, the average age of extraction from the depleted mantle was between 1.38 and 0.94 Ga (Fig. 6a), with no clear trend with time throughout the Late Triassic (Fig. 6a). These data suggest that the Late Triassic magmatism of the Antarctic Peninsula predominantly recycled crustal components that were initially derived from juvenile Mesoproterozoic to Neoproterozoic crust. The timing of melt extraction from the depleted mantle reservoir approximately coincides with the temporally protracted Sunsas belt of South America (1.19–0.92 Ga; Cordani and Sato, 2000) and the Grenville-age crust of East Antarctica (1.1–1.0 Ga; Goodge and Fanning, 2016), which has been already found in West Antarctica (Nelson and Cottle, 2018). Therefore, the Late Triassic orthogneisses in Antarctic Peninsula may host the precursor components of a Sunsas- or Greville-aged crust.

### *5.2. Inherited zircon cores in Triassic magmas: Eastern Domain vs Central Domain*

#### *5.2.1. Palaeozoic*

The $^{206}Pb/^{238}U$ concordia ages of zircon cores (located using cathodoluminescence) within seven Late Triassic alkali granites, syenogranites and quartz-syenites show clear differences between the Central and the Eastern domains (Fig. 7; see also Fig. 6c). Zircon core ages from the Central Domain record almost continuous magmatism/metamorphism from 253 ± 2 Ma to the Cambrian (~530 Ma), and two zircons yield Neoproterozoic ages of 770 ± 8 and 751 ± 6 Ma (Fig. 4g and 7). $\varepsilon Hf_t$ values of the Permian to Silurian zircon cores in the Central Domain span between −5.3 to 4.9, and follow a rough trend towards less radiogenic values as they become younger (Fig. 6c). The Lu—Hf model ages of the cores and Triassic zircon rims in the Central Domain yield ages of 1.38 to 0.73 Ga (Fig. 10), suggesting that a majority of the precursor crustal rocks formed part of a Sunsas-aged belt. These data suggest the crustal sedimentary and igneous

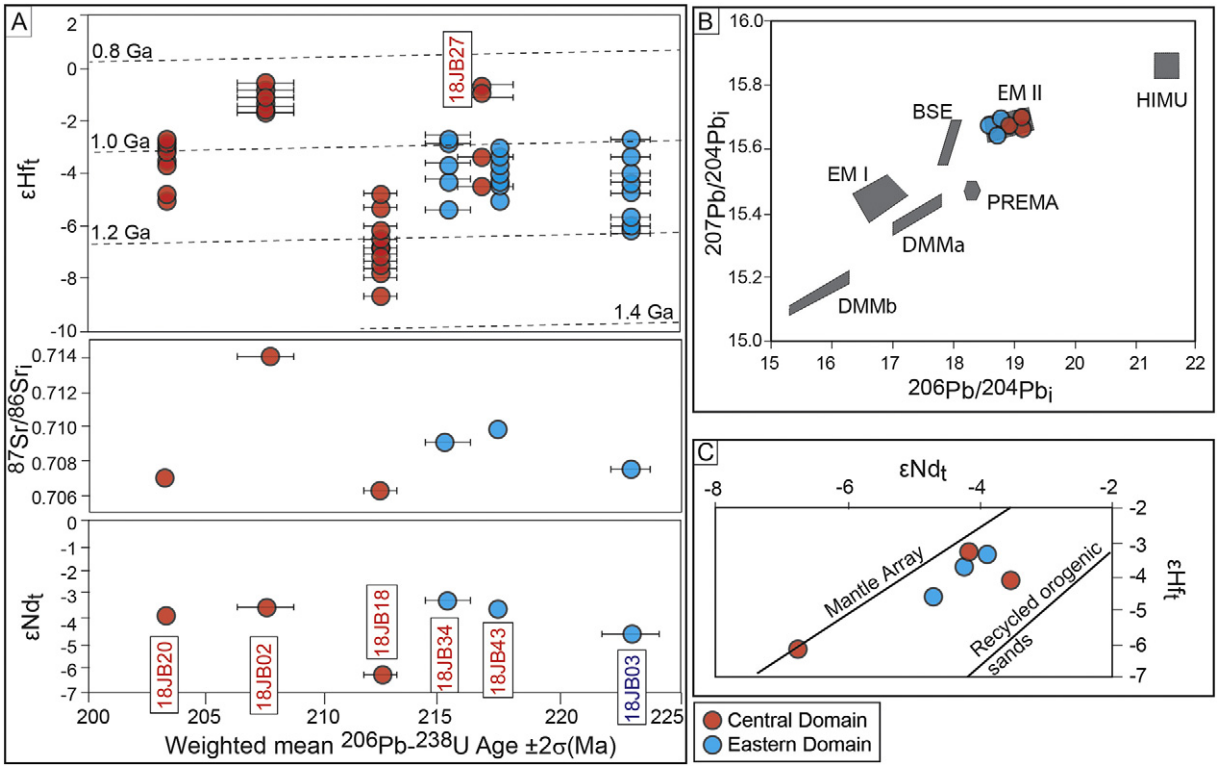


**Fig. 9.** (A) Graphical summary of isotopic data collected during this study from Triassic orthogneisses, showing the temporal evolution of zircon $\varepsilon Hf_t$, and whole rock $^{87}Sr/^{86}Sr_i$ and $\varepsilon Nd_t$. Dashed lines correspond to the crustal evolution of the Lu—Hf isotopic system with an average crustal $^{176}Lu/^{177}Hf$ ratio of 0.0113 (Gerdes and Zeh, 2006 and references therein), and are labelled according to their corresponding model age. (B) Initial Pb-isotopic ratios showing the classification fields of Zindler and Hart (1986); EM I: enriched mantle with recycled lower continental crust, EM II: enriched mantle with upper continental crust and continental derived sediments, PREMA: prevalent mantle composition, BSE: bulk silicate earth, HIMU: high U/Pb mantle composition, DMMa: depleted MORB-mantle with isotopic radiogenic enrichment, DMMn: depleted MORB-mantle with isotopically depleted enrichment. (C) A comparison of $\varepsilon Hf_t$ (weighted mean value in the Triassic zircon rims) vs. $\varepsilon Nd_t$ (whole rock). Regressions for the Mantle Array and Recycled Orogenic Sands are from Vervoort et al. (1999).

source rocks that melted to form the Triassic magmas in the Central Domain are likely to have formed part of the Permian to Cambrian continental arcs, which are preserved along extensive regions of the relict Terra Australis margin of Gondwana (Cawood, 2005), although these have not been previously extensively identified in the Antarctic Peninsula (e.g. Riley et al., 2012b; Nelson and Cottle, 2017, 2018). Examples of Gondwanan Palaeozoic continental arcs are exposed in Chile and Argentina (e.g. Otamendi et al., 2012; Castillo et al., 2017; Hervé et al., 2016), Peru (e.g. Chew et al., 2007; Mišković et al., 2009), Colombia and Venezuela (Villagomez et al., 2011; van der Lelij et al., 2018), and Australia (Foster et al., 2009, Cawood et al., 2011), and we propose that these arcs extended into the crust of the Central Domain of the present day Antarctic Peninsula (Fig. 11). $\varepsilon Hf_t$ values from the Ordovician – late Cambrian continental arc exposed in Colombia and Venezuela range between 4.5 and 0.1 (van der Lelij et al., 2018; Fig. 10b), with Lu—Hf model ages ranging between 1.57 and 0.82.

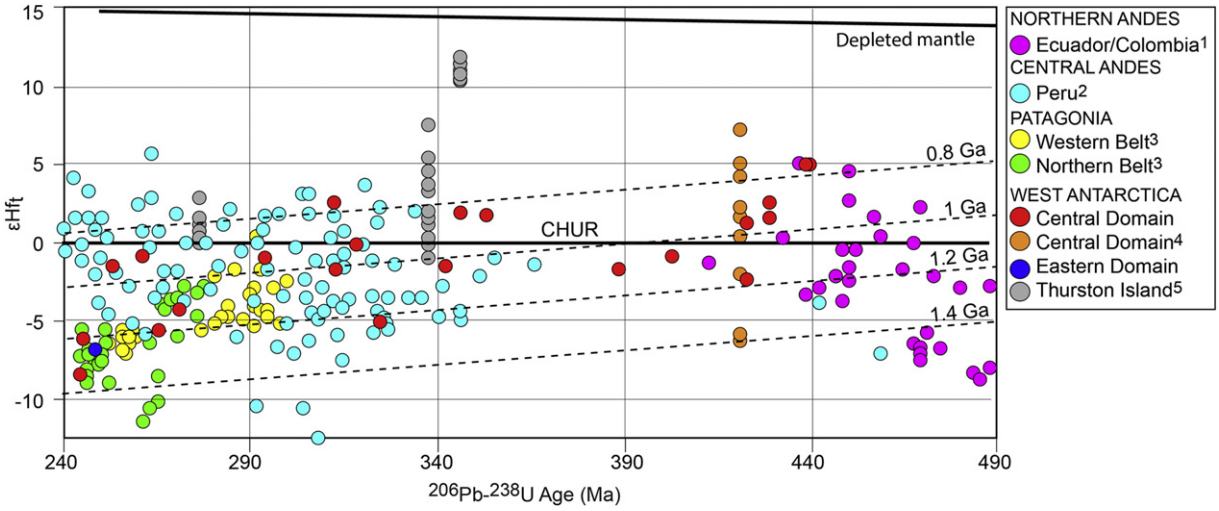


**Fig. 10.** Zircon $\varepsilon Hf_t$ values from Palaeozoic and Mesozoic arc rocks of the South American and West Antarctic segments of the Terra Australis Margin. Dashed lines are calculated using an average crustal $^{176}Lu/^{177}Hf$ ratio of 0.0113 (Gerdes and Zeh, 2006 and references therein) for various model ages. The comparison includes data acquired in this study (Central and Eastern Domain), along with data from 1) van der Lelij et al. (2018), 2) Mišković and Schaltegger (2009), 3) Castillo et al. (2017), 4) Flowerdew et al. (2006), and 5) Nelson and Cottle (2018).

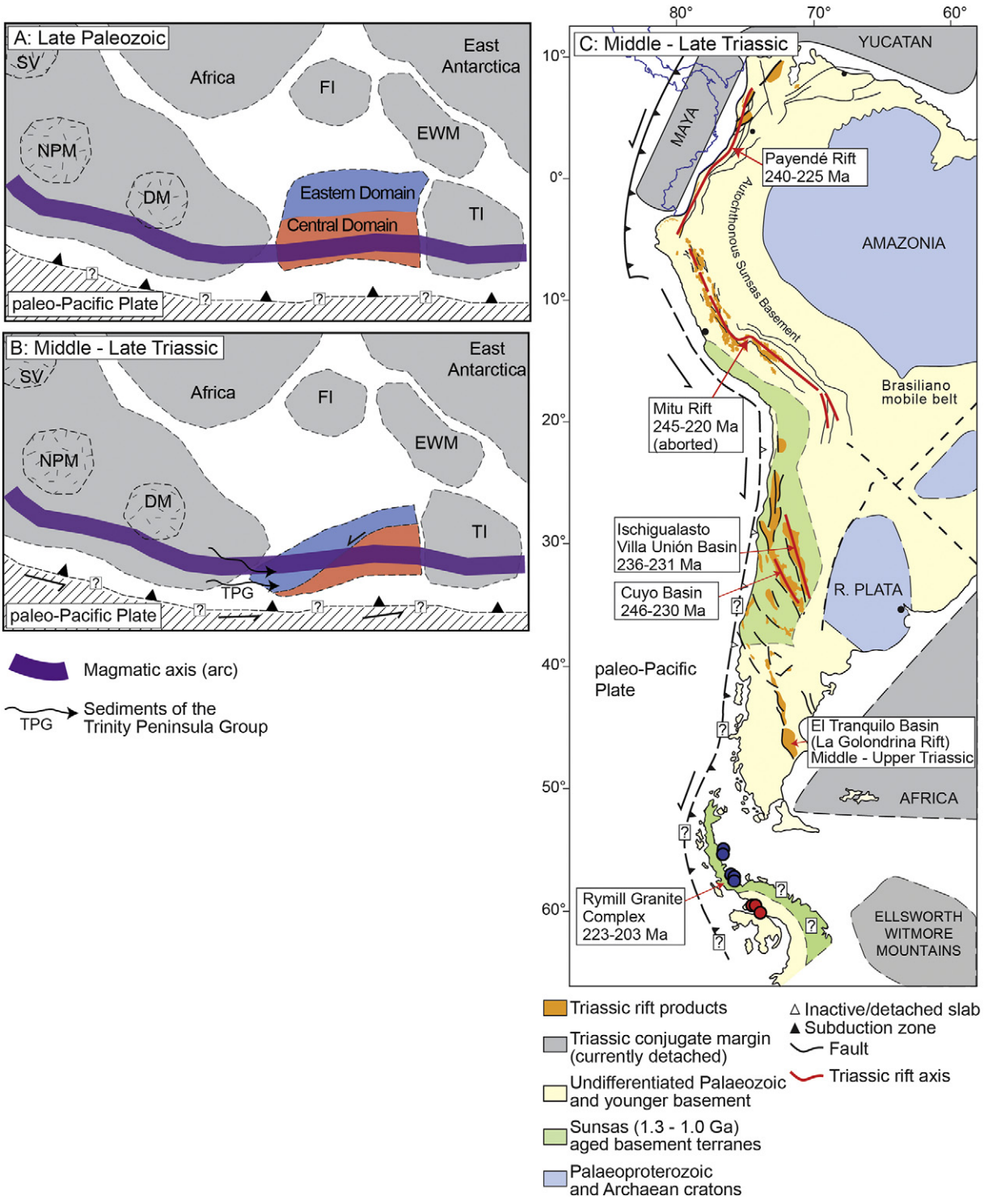


**Fig. 11.** (A) Schematic late Palaeozoic reconstruction of southwestern Gondwana showing the subduction of Palaeo-Pacific oceanic lithosphere in the South America–Patagonia-Antarctica sector (modified from Castillo et al., 2017). The Eastern Domain (blue) is distal from the active margin and beyond the magmatic reach of the Palaeozoic arc. An Early Neoproterozoic zircon core suggests it may have been modified by Sunsas-aged orogenesis. The Central Domain (red) is located proximal to the long-lived active margin, and was modified by arc magmatism. (B) Schematic Middle- Late Triassic reconstruction of southwestern Gondwana showing a dominant sinistral transtensional regime that displaced the Eastern Domain into the Triassic arc axis. (C) Simplified illustration of the distribution of Triassic extensional basins and rifts, and associated sedimentary and igneous rocks along western South America during the Middle–Late Triassic (from Spikings et al., 2016). Age ranges shown are from zircon U—Pb concordia ages of detrital zircons, volcanic rocks and peralluminous intrusions (citations listed in Spikings et al., 2016). The position of the Antarctic Peninsula is taken from the palaeogeographic reconstructions of Grunow et al. (1991) and König and Jokat (2006). DM: Deseado Massif, EWM, Ellsworth–Whitmore Mountains block, FI: Falkland Islands, NPM: North Patagonian Massif, TI: Thurston Island, SV: Sierra Verde.

Palaeozoic arc rocks in Peru span between Permian to late Cambrian Ma, and yield $\varepsilon Hf_t$ and Lu—Hf model ages ranging between −12.5 and 5.6, and 1.4–0.70 Ga, respectively (Fig. 10; Mišković and Schaltegger, 2009), which overlap with data obtained from the Central Domain. Finally, Palaeozoic continental arc rocks from Patagonia (Fig. 11) yield zircon U—Pb concordia ages of 254 ± 3 to 294 ± 2 Ma (Pankhurst et al., 2006; Castillo et al., 2017) from zircon rims, while cores ages span between 245 ± 3 to 541 ± 8 Ma, and yield $\varepsilon Hf_t$ values that span

between 4.7 and −14.7, with Lu—Hf model ages of 0.92–2.12 Ga (Fig. 10, Castillo et al., 2017). These time periods of continental arc activity along western Gondwana, within Pangaea, temporally overlap with the age of xenocrystic zircon cores in the Central Domain, while the Hf (zircon) isotopic compositions also fairly overlap (Fig. 10), supporting a hypothesis that the Palaeozoic xenocrystic cores in the Central domain were derived by solid-state reworking and incorporated in the magmas of the same arc.

Only two Palaeozoic zircon cores were obtained from Late Triassic plutons exposed in the Eastern Domain (Fig. 7), and these were obtained from orthogneiss 18JB03 (258.9 ± 8.0 Ma; this study) and granodioritic gneiss R.2602.1 (497 ± 6 Ma; Flowerdew et al., 2006). These xenocrystic zircons were either incorporated via the melting of sedimentary units that were sourced from Palaeozoic arc crust in the Central Domain, or via re-melting of Palaeozoic intrusions.

#### 5.2.2. Neoproterozoic

Two concordant $^{206}Pb/^{238}U$ zircon core ages of 751 ± 6 and 770 ± 8 Ma in a quartz-syenite (18JB27, Fig. 4g) of the Central Domain post-date the amalgamation of Rodinia, and Sunsas-aged metamorphism and magmatism. Potential source regions are scarce within West Gondwana and Laurentia, although they may be derived from rift-related magmatism located along the Eastern Laurentian margin (Hoffman, 1991; Dalziel, 1991; Meert and Torsvik, 2003) in the southern Appalachians, and within the Precordillera Terrane (774 ± 6 Ma; Baldo et al., 2006), Eastern Cordillera of Peru (e.g. 752–691 Ma; Chew et al., 2007; Mišković et al., 2009), Patagonia (e.g. inherited zircons in the Somuncura Massif; Ramos and Naipauer, 2014), and East Antarctica (e.g. inherited cores in the Sør Rondane Mountains; Osanai et al., 2013).

Early and Late Neoproterozoic zircon cores are more abundant in the Eastern Domain (Fig. 7), with ages of 1055 ± 8, 966 ± 21, 607 ± 7, and 580 ± 13 Ma. These ages span a period of time that is poorly defined in our study due to the low quantity of data, although they are typical of Rodinian and Gondwanan provinces. They are probably derived from Sunsas (~1.19–0.92 Ga; Cordani and Sato, 2000) and Brasiliano-aged orogens (~700–500 Ma; e.g. Brito-Neves and Cordani, 1991). The $\varepsilon Hf_t$ values of the Neoproterozoic zircon xenocrysts in the Eastern Domain reveal a tendency towards less radiogenic sources with younger ages during ~1050–580 Ma (Fig. 7), although the dataset is small and this trend may not be representative. Regardless, the Hf isotopic compositions of the Triassic zircons reveal a consistent array of Lu—Hf model ages that vary from 1.29 to 1.05 Ga (Fig. 10), suggesting that the late Neoproterozoic anatectites (Lu—Hf model ages between 1.33 and 1.04 Ga) formed by melting of Sunsas-aged source rocks (e.g. Cordani and Sato, 2000), while the early Neoproterozoic xenocrysts (Lu—Hf model ages between 1.18 and 0.90 Ga) may represent relict components of a Sunsas-aged, isotopically juvenile province. The paucity of Palaeozoic zircons, combined with a greater prevalence of Neoproterozoic zircons in the Eastern Domain compared to the Central Domain, suggests the Eastern Domain may have occupied a more internal position within Gondwana, located proximal to or part of a Braziliano or Sunsas-aged belt.

Summarising, all of the Triassic crustal magmatic components were originally derived from orogens that formed during the amalgamation of Rodinia during 1.3–0.9 Ga (herein referred to as Sunsas-aged), with a potential minor contribution from magmatic units that formed during the early stages of breakup of Rodinia. Some of these zircons were directly incorporated into Triassic magmas in the Eastern Domain. However, a majority of the Sunsas-aged component was re-melted and incorporated into Palaeozoic arcs that formed along the Terra Australis margin of Gondwana, and then incorporated into Triassic magmas in the Central Domain via solid-state reworking of zircons.

## 6. Discussion

### 6.1. Palaeozoic: An active margin in the Antarctic Peninsula, and the relative positions of the Central and Eastern Domain

A plethora of zircon xenocrystic cores that crystallised between 528 ± 6 to 259 ± 5 Ma in Late Triassic orthogneisses in northwestern Palmer Land suggests that the Central Domain of Vaughan and Storey (2000) may have been located along an active margin during the late Cambrian – Permian period. With the exception of spatially restricted exposures of Ordovician gneisses at Target Hill and Eden Glacier (Milne and Millar, 1989; Riley et al., 2012b; Fig. 2), there is limited direct evidence for a Palaeozoic basement in the Antarctic Peninsula. However, given that the Late Triassic rocks were derived by melting of igneous and sedimentary precursors that probably formed within an arc, we suggest that large regions of the Central Domain may host buried Palaeozoic igneous and sedimentary rocks. This is consistent with the extensive evidence indicating the development of an active margin at the western margin of Pangea during the Palaeozoic. Prior to the Triassic, the proto–Antarctic Peninsula is considered to have been located somewhere along the southwestern margin of Pangea, south of Patagonia and north of Thurston Island, (e.g. Grunow et al., 1991; Ghidella et al., 2002; Dalziel and Elliot, 1982; Fig. 11), both of which host middle and late Palaeozoic magmatic rocks. Nelson and Cottle (2017, 2018) used zircon geochronology and isotopic tracing to show that western Gondwana hosted an episodically active margin through most of the Palaeozoic, and they proposed the existence of two tectonic domains. These domains are i) South America – Antarctic Peninsula – Thurston Island, and ii) Marie Byrd Land – Australia – Zealandia. Furthermore, Carboniferous orthogneisses are exposed within the Thurston Island block (Riley et al., 2017b), while Ordovician – Permian arc related plutons are found in southern South America (e.g. Rapela et al., 2018; Ramos, 2008; Pankhurst et al., 2006). The Palaeozoic magmatic record of the Thurston Island block can be divided into i) Carboniferous magmatism and metamorphism that formed granitic gneisses (~349–309 Ma U-Pb zircon and Rb—Sr whole-rock dates; Riley et al., 2017b, Pankhurst et al., 1993), and was coeval with magmatism in Marie Byrd Land and New Zealand (~396–338 Ma; Scott et al., 2009; based on U—Pb zircon dates), and ii) Late Carboniferous – Late Triassic mafic magmatism (~310–230 Ma; K—Ar and $^{40}Ar/^{39}Ar$ dates; Pankhurst et al., 1993). Palaeozoic magmatic and metamorphic events in Patagonia include i) the Pampean Orogeny (~552–520 Ma; Casquet et al., 2018), which occurred in response to the assembly of southwestern Gondwana (e.g.; Casquet et al., 2018), ii) Early Ordovician magmatism associated with the Famatinian Orogeny (~486–463 Ma, e.g. Rapela et al., 2018), which is widespread and extends northwards along the Pacific margin of South America towards Venezuela (e.g. Chew et al., 2007; van der Lelij et al., 2018; Pankhurst et al., 2006), iii) Devonian magmatism at the northwestern margin of Patagonia, related to the initiation of subduction of the proto–Pacific plate (~391–361 Ma; Hervé et al., 2016), and iv) Permian magmatism that formed arcs along the northern and western margins of Patagonia (~294–246 Ma; e.g. Castillo et al., 2017 and references therein; Fig. 10). Recent studies of the geochronological and geochemical in plutonic rocks in southern Patagonia proposed there was an active margin related to a flat slab during the Late Triassic period (Navarrete et al., 2019; Suárez et al., 2019).

Punctuated magmatism spanning between the Early Ordovician and Permian within Patagonia and the Thurston Island block was synchronous with that observed in the Central Domain, and thus we suggest that Palaeozoic arc magmatism also modified continental crust of the Central Domain, and formed above a common subduction zone. Therefore, the basement of the Central Domain (as defined by Vaughan and Storey, 2000) is at least as old as ~527 Ma, which is the oldest zircon core obtained from the Central Domain (granite 18JB27), while Target Hill probably represents an inlier of the basement sequence that is significantly more extensive in the subsurface. Furthermore, the north-

south orientation of the Western Margin Arc of Patagonia, which was active from the Devonian to the Cretaceous (e.g. Ramos, 2008; Nelson and Cottle, 2018; Navarrete et al., 2019), fits well with a northward continuation of a late Palaeozoic arc in the Antarctic Peninsula (Fig. 11) when using the reconstruction of König and Jokat (2006) for this period.

Given that the Triassic plutons formed by melting both igneous and sedimentary sources, we would expect to find Palaeozoic zircons within the fore- and backarc regions of the Palaeozoic arc. However, we only found one Late Permian zircon core (259 ± 5 Ma) within Triassic plutons in the Eastern Domain, which may have resided in sedimentary source rocks. Therefore, we consider the Eastern Domain to have been distal to the main Palaeozoic arc, and it is likely that it was located further within the interior of Gondwana (Fig. 11).

Lu—Hf model ages for the Triassic zircon rims, and Palaeozoic and late Neoproterozoic zircon cores in the Central Domain span between 1.24 and 0.73 Ga. The primordial continental crust was at least 500–900 million years old prior to one or more anatectic cycles, and eventually formed Palaeozoic arc crust along the Terra-Australis margin. The primordial crust probably formed part of a Sunsas-aged belt, and thus it is likely that Sunsas-aged rocks either form the basement to the Central Domain, or were located inboard of it during the Palaeozoic within Gondwana. The lack of Neoproterozoic zircon cores in the Central Domain (Fig. 7) may be due to efficient re-melting during Palaeozoic magmatism, which did not affect the Eastern Domain. Similar $^{206}Pb/^{238}U$ zircon and Lu—Hf ages of some zircon cores, e.g. 966 ± 21 Ma and 1.18 Ga, respectively (alkali granite, 18JB03) in the Late Triassic orthogneisses of the Eastern Domain suggests they are juvenile crustal components, which were not affected by magmatism along the Terra Australis margin. Therefore, it is plausible to suggest that the basement of the Eastern Domain may be Sunsas-aged, and thus may have originally formed part of the several thousand kilometer long orogenic belt that currently rims the entire southern margin of the Zimbabwe-Kaapvaal-Grunehogna craton, and extends into Dronning Maud Land in East Antarctica (e.g. Jacobs et al., 2003).

### 6.2. Triassic: Tectonic setting

The Triassic magmatic rocks (Rymill Granite Complex) are characterised as: i) gneissic, high-K calc-alkaline syenogranites and alkali granites, ii) enriched LILE and LREE with negative Nb, Ta, Sr and Ti anomalies, iii) isotopically evolved relative to CHUR, iv) no mafic rocks, and v) unlike the Palaeozoic arc, they occur in both the Central and Eastern domains of Vaughan and Storey (2000). We acknowledge that there is a paucity of data, which is a direct consequence of sampling rocks in remote regions of Antarctica. Nevertheless, these observations support an active arc setting with mixed igneous and sedimentary source rocks. We are unable to use our data to distinguish between a compressional or extensive setting, although the lack of bimodality does not support extensive thinning of the continental lithosphere. The Antarctic Peninsula was located south of Patagonia and north of the Thurston Island block during the Triassic (Fig. 11; e.g. Hervé et al., 2006b; König and Jokat, 2006). Although there is a paucity of data about the Triassic history of the Thurston Island block, similar geodynamic behavior has been shown by regional studies of Patagonia-Antarctic Peninsula-Thurston Island during the Mesozoic (Navarrete et al., 2019; Pankhurst et al., 2000; Riley et al., 2001) and late Palaeozoic (Nelson and Cottle, 2017, 2018) periods, and thus here we propose a potential tectonic setting for the Antarctic Peninsula via comparisons with Patagonia and the Pacific margin in South America (Fig. 11).

The entire Pacific margin of South America was under extension during 245–220 Ma (Spikings et al., 2016). North of the Huancabamba Deflection (5°S) along the Pacific coast of South America, the Triassic is characterised by tholeiitic mafic lavas and metamorphosed, peraluminous S-type crustal anatectites that were emplaced during a rift to drift transition (Payendé Rift; Spikings et al., 2016; Fig. 11). Continental rifting during 240–225 Ma separated parts of the basement of Mexico and Guatemala from western Pangaea, forming ophiolites by 216 Ma (Spikings et al., 2016). Rifting is considered to have been accompanied by sinistral shearing (Litherland et al., 1994) within a back-arc (Cochrane et al., 2014; Spikings et al., 2015). Further south, concordant zircon U—Pb ages of lavas and tuffs, combined with U—Pb concordia ages obtained from detrital zircons in sedimentary strata constrain the age of the Mitu Group in Peru to ~245–220 Ma, and constrains the time of Middle – Late Triassic extension (Mitu Rift; Spikings et al., 2016; Fig. 11). Finally, a series of Middle – Late Triassic rift systems and sinistral pull-apart basins (e.g. Cuyo, Ischigualasto-Villa Unión Basin) with a NNW-SSE trend in northern and central Chile and Argentina (Charrier, 1973) propagated along the hanging wall of previous sutures that separate Palaeozoic terranes (e.g. Ramos and Kay, 1991; Ramos, 1994). Maksaev et al. (2014) compile and present new zircon U—Pb dates from volcanic rocks in northern Chile, which reveals a peak in activity between 240 and 202 Ma. The Middle – Late Triassic volcanic rocks are associated with coeval post-orogenic, peraluminous intrusions and bimodal magmatism (e.g. Martin et al., 1999) in the high Chilean Andes and Coastal Cordillera, which yield zircon U—Pb dates that peak between 247 and 216 Ma in northern Chile (Maksaev et al., 2014). Recently, Triassic igneous rocks in Central Chile have been interpreted to be subduction-related (González et al., 2018; Coloma et al., 2017; Espinoza et al., 2019; del Rey et al., 2016, 2019). Further, Navarrete et al. (2019) utilised geochemical and geochronological data to propose a flat-slab active margin for the Triassic period in Patagonia.

Late Triassic back-arc plutons in the Acatlán Complex (Mexico; Helbig et al., 2012) were utilised by Cochrane et al. (2014) and Spikings et al. (2015) to propose that subduction drove rifting along northwestern South America, which was also proposed by Pindell and Tabbutt (1995). In contrast, no clear evidence exists for subduction along the Peruvian margin between 240 and 210 Ma, and slab-pull forces do not seem to account for Middle-Late Triassic extension in Peru and Bolivia (Spikings et al., 2016). Spikings et al. (2016) account for plate-margin wide sinistral-directed stress, a paucity of subduction south of the present-day Huancabamba Deflection, and coeval subduction to the north by suggesting that oceanic lithosphere of the eastern Pacific Ocean displaced with a southward component along the entire margin, driving transtension and the opening of rift basins. Alternatively, other authors hypothesized that extension along the Chilean margin was driven by slab detachment (e.g. Mpodozis and Ramos, 1989; Kay et al., 1989; Franzese and Spalletti, 2001), or lithospheric delamination (Ramos, 2009) or by slab-steepening above an active subduction zone (Ramos and Kay, 1991; Vasquez et al., 2011).

Late Triassic magmatism affected both the Central and Eastern domains of Vaughan and Storey (2000), whereas Palaeozoic magmatism appears to have mainly only modified the Central Domain. Therefore, we speculate that Triassic transtension along the Pacific margin drove oceanward displacement of the Eastern Domain relative to its Palaeozoic location within Pangaea, juxtaposing it against the Central Domain and placing them both within the zone of arc magmatism (Fig. 11b). Triassic magmatism in the Eastern Domain (237–215.2 Ma) slightly predates that in the Central Domain (228–203.3 Ma; Fig. 6a). Rift sedimentation and magmatism terminated during ~216–209 Ma in Colombia, Ecuador, Peru and northern Chile, coinciding with the onset of subduction in those regions (Boekhout et al., 2013; Casquet et al., 2014; Spikings et al., 2015) and the initiation of the so-called Andean Cycle (Fig. 11c). This time period is consistent with the termination of Triassic magmatism within the Antarctic Peninsula (~203 Ma), and it may reveal a slight younging and reduction of extensional forces from South America to the Antarctic Peninsula, accounting for the lack of Triassic, mafic tholeiitic rocks. Few geochemical datasets have been reported from Jurassic plutonic rocks in the Antarctic Peninsula, although a comparison between the major oxides and trace element compositions of Jurassic (Bastias et al., 2017) and Triassic (this study)

granitoids reveals no significant differences. This might be explained with a weaker Triassic extension of the continental lithosphere of the Antarctic Peninsula compared to other regions of the Terra Australis margin located within South America, and unlike a significant section of the South American margin (e.g. Spikings et al., 2016), there may have been continuous subduction beneath the Antarctic Peninsula from ~223 Ma into the Jurassic. Further, this would corroborate recent studies that propose the existence of an active margin along the Chilean margin (del Rey et al., 2016, 2019; Oliveros et al., 2018; Espinoza et al., 2019), includingPatagonia (Navarrete et al., 2019; Suarez et al., 2019).

U—Pb concordia ages of zircons within metasedimentary rocks of the Trinity Peninsula Group (Eastern Domain; Fig. 2) suggest it was deposited during the Permian – Triassic (e.g. Barbeau et al., 2010; Hervé et al., 2006b), which are consistent with fossil evidence for Triassic deposition (Thomson, 1975). Provenance studies (U—Pb zircon ages and dense minerals) reveal a dominant Permian igneous source (e.g. Fanning et al., 2011), with a likely tonalitic-granodioritic average composition (Castillo et al., 2015). The geological setting of the Trinity Peninsula Group is not clear, and interpretations range from an accretionary complex (e.g. Dalziel, 1984) to an upper slope basin setting (e.g. Smellie, 1991). These observations are consistent with deposition along an active margin in a slope-apron setting during the Permian – Triassic. Although the detrital age pattern in these sedimentary rocks reveals a consistent abundance of Permian ages (e.g. Fanning et al., 2011), significant trench-parallel differences are found in the abundance of late- and middle Palaeozoic zircons (e.g. Castillo et al., 2016). Northern exposures of the Trinity Peninsula Group (~63°S) host a relatively large abundance of Cambrian – Carboniferous zircons compared to the south (~65°S e.g. Castillo et al., 2016). We hypothesise that the leading edge of the Eastern Domain became a depocenter for Early Palaeozoic detritus during the approximate Triassic, sinistral, trench-parallel displacement of the Eastern Domain relative to the Central Domain (Fig. 11b). The source regions of the Early Palaeozoic detritus were located in the Central Domain and southern South America. Subsequent sinistral displacement progressively brought the Eastern Domain into the Triassic active margin, which had mainly buried the Palaeozoic basement of the Central Domain prior to the arrival of more interior regions of the Eastern Domain, starving it of Early Palaeozoic detritus. This deformation probably occurred along the Eastern Palmer Land Shear Zone, accommodating the relative movements of the Central and Eastern Domains.

Relative displacement between the Eastern and Central Domains of the Antarctic Peninsula during the Triassic supports the model of Vaughan and Storey (2000) to the extent that they may have formed in separate locations. However, given that Palaeozoic and Triassic zircons from both regions consistently yield Sunsas-aged model Lu—Hf ages, we propose that they both originated within Gondwana and the primordial crustal rocks formed during the amalgamation of Rodinia. Juxtaposition of the Eastern and Central domains occurred in the Triassic, and thus we speculate that the Eastern Palmer Land Shear Zone originally formed in the Triassic during transtension along the Pacific margin.

## 7. Conclusions

A Palaeozoic magmatic arc is recorded in zircon cores in Triassic plutons in the Antarctic Peninsula. Palaeozoic $^{206}Pb/^{238}U$ zircon concordia ages span between 253 ± 2 and 528 ± 6 Ma, and with the exception of one zircon in the Eastern Domain that yields a concordant age of 259 ± 5 Ma, they are mainly found within the Central Domain as defined by Vaughan and Storey (2000). We equate these Palaeozoic zircons from the Central Domain with the well-studied Palaeozoic arcs that formed along the Terra Australis Margin of South America, and spanned from Venezuela to the Antarctic Peninsula. We interpret the paucity of evidence for Palaeozoic magmatism in the Eastern Domain as a consequence of a further interior position within Pangaea, distal from the main axis of arc magmatism. Lu—Hf model ages of the Palaeozoic zircon cores in the Central Domain range between 1.24 and 0.81 Ga, while model ages of late Neoproterozoic cores (~579–604 Ma) in the Eastern Domain are only ~ 500 Ma older than their zircon U—Pb concordia ages. Therefore, we suggest that the basement of the Antarctic Peninsula consists of a Palaeozoic arc, which may have re-melted Sunsas-aged rocks that represent relict parts of Rodinia and possibly form the deep crust of the Eastern Domain.

High-K calc alkaline magmas of the Rymill Granite Complex intruded the Central and Eastern domains of Vaughan and Storey (2000) during 217–203 Ma and 223–215 Ma, respectively. The source rocks included igneous and sedimentary crustal material which formed by crustal reworking of Sunsas-aged rocks during middle Neoproterozoic extension, Braziliano-aged orogenesis, and Palaeozoic arc magmatism. Sinistral transtension prevailed along western Gondwana (within Pangaea) during the Triassic, which juxtaposed the Central and Eastern Domains within the Triassic arc, and drove oceanward migration of the arc. We suggest that the Late Triassic magmas in both domains formed above an active subduction zone, which may have continued into the Jurassic. We speculate that the amount of lithospheric extension diminished traversing southwards along the Pacific margin of South America, towards the Antarctic Peninsula. This reduction is manifested as a transition from a rift-to-drift transition in Colombia and Ecuador, to failed rifts in Peru and Argentina, to transtension and the disappearance of bimodal magmatism in the Antarctic Peninsula.

We propose that the Central and Eastern Domains originated proximal to or within Sunsas-aged belts of Rodinia. The Eastern Domain was located inboard of the Central Domain throughout the Palaeozoic, beyond the reach of Palaeozoic arc magmatism. The domains were juxtaposed during Triassic sinistral transtension along the South American-West Antarctic sectors of the Terra Australis margin. Sinistral displacement formed the Eastern Palmer Land Shear Zone, which remained as a long-lived structural weak zone in West Antarctic crust (e.g. Vaughan and Storey, 2000).

## Declaration of competing interest

The authors declare that they have no known competing financial interests or personal relationships that could have appeared to influence the work reported in this paper.

## Acknowledgements

The authors are grateful for the extensive logistical support provided by the Chilean Antarctic Institute (INACH) during two field campaigns to the Antarctic Peninsula. We thank the British Antarctic Survey who provided access to their sample archive, with the donation of rocks for this study. Support was provided by the staff and laboratories of the Isotope Geochemistry Group of the University of Geneva. This Project was funded by the Chilean Antarctic Institute project RT-06-14 and the University of Geneva. J.B. has been supported by a CONICYT - Chile scholarship, Earth Science Department of the University of Geneva and the Schmidheiny Foundation at Switzerland. Andrea Festa is thanked for editorial handling, and the authors are grateful to Veronica Oliveros, Victor Ramos and an anonymous reviewer for providing constructive criticism which improved the manuscript.

## References

Aitkenhead, N., 1975. The geology of the Duse Bay-Larsen Inlet area, North-East Graham Land. Brit. Antarct. Surv. Sci. Rep. 51, 62.

Albarède, F., Telouk, P., Blichert-Toft, J., Boyet, M., Agranier, A., Nelson, B., 2004. Precise and accurate isotopic measurements using multiplecollector ICPMS. Geochim. Cosmochim. Acta 68, 2725–2744.

Augustsson, C., Willner, A.P., Rüsing, T., Niemeyer, H., Gerdes, A., Adams, C.J., Miller, H., 2016. The crustal evolution of South America from a zircon Hf-isotope perspective. Terra Nova 28, 128–137. https://doi.org/10.1111/ter.12200.

Baker, J., Peate, D., Waight, T., Meyzen, C., 2004. Pb isotopic analysis of standards and samples using a 207Pbe204Pb double spike and thallium to correct for mass bias with a double-focusing MC-ICP-MS. Chem. Geol. 211 (3e4) (275e303).

Baldo, E., Casquet, C., Pankhurst, R.J., Galindo, C., Rapela, C.W., Fanning, C.M., Dahlquist, J., Murra, J., 2006. Neoproterozoic A-type magmatism in the western Sierras Pampeanas (Argentina): evidence for Rodinia break-up along a proto-Iapetus rift? Terra Nova 18, 388–394.

Balgord, E.A., 2017. Triassic to Neogene evolution of the south-central Andean arc determined by detrital zircon U-Pb and Hf analysis of Neuquén Basin strata, central Argentina (34°S–40°S). Lithosphere 9, 453–462. https://doi.org/10.1130/L546.1.

Barbeau, D.L., Davis, J.T., Murray, K.E., Valencia, V., Gehrels, G.E., Zahid, K.M., Gombosi, D.J., 2010. Detrital-zircon geochronology of the metasedimentary rocks of north-western Graham Land. Antarct. Sci. 22, 65. https://doi.org/10.1017/S095410200999054X.

Bastias, J., Hervé, F., 2013. The Cape Wallace Beds: a Permian-detritus turbidite unit at Low Island, South Shetland Islands: Bollettino Di Geofisica Teorica EdApplicata. Supplement 2. 54, 312–314.

Bastias, J., Spikings, R., Ulianov, A., Schaltegger, U., Grunow, A., Hervé, F., 2017. Mesozoic to Cenozoic U-Pb zircon ages from Graham Land, West Antarctica: the magmatic evolution of the Antarctic Peninsula batholith. 19th EGU General Assembly, EGU2017, Proceedings from the Conference Held 23–28 April, 2017 in Vienna, Austria, p. 17260.

Bastias, J., Calderon, M., Israel, L., Herve, F., Spikings, R., Pankhurst, R., Castillo, P., Fanning, M., Ugalde, R., 2019a. The Byers Basin: Jurassic-Cretaceous tectonic and depositional evolution of the forearc deposits of the South Shetland Islands and its implications for the northern Antarctic Peninsula. Int. Geol. Rev. https://doi.org/10.1080/00206814.2019.1655669.

Bastias, J., Spikings, R., Ulianov, A., Chiaradia, M., Baumgartner, L., Bouvier, A.S., 2019b. Data for: the Gondwanan margin in West Antarctica: insights from Late Triassic magmatism of the Antarctic Peninsula. Mendeley Data v5. https://doi.org/10.17632/d3dn852ph3.5.

Béguelin, P., Chiaradia, M., Beate, B., Spikings, R., 2015. The Yanaurcu volcano (Western Cordillera, Ecuador): a field, petrographic, geochemical, isotopic and geochronological study. Lithos 218, 37–53.

Black, L.P., Kamo, S.L., Allen, C.M., Davis, D.W., Aleinikoff, J.N., Valley, J.W., Mundil, R., Campbell, I.H., Korsch, R.J., Williams, I.S., Foudoulis, C., 2004. Improved Pb-206/U-218 microprobe geochronology by the monitoring of a trace-elementrelated matrix effect; SHRIMP, ID-TIMS, ELA-ICP-MS and oxygen isotope documentation for a series of zircon standards. Chem. Geol. 205, 115–140.

Boekhout, F., Spikings, R., Sempere, T., Chiaradia, M., Ulianov, A., Schaltegger, U., 2012. Mesozoic arc magmatism along the southern Peruvian margin during Gondwana breakup and dispersal. Lithos 146–147, 48–64.

Boekhout, F., Sempere, T., Spikings, R., Schaltegger, U., 2013. Late Paleozoic to Jurassic chronostratigraphy of coastal southern Peru: temporal evolution of sedimentation along an active margin. J. S. Am. Earth Sci. 47, 179–200.

Bouvier, A., Vervoort, J.D., Patchett, P.J., 2008. The Lu–Hf and Sm–Nd isotopic composition of CHUR: constraints from unequilibrated chondrites and implications for the bulk composition of terrestrial planets. Earth Planet. Sci. Lett. 273, 48–57.

Bradshaw, J.D., Vaughan, A.P.M., Millar, I.L., Flowerdew, M.J., Trouw, R.A.J., Fanning, C.M., Whitehouse, M.J., 2012. Permo–Carboniferous conglomerates in the Trinity Peninsula Group at View Point, Antarctic Peninsula: sedimentology, geochronology and isotope evidence for provenance and tectonic setting in Gondwana. GeologicalMagazine 149 (4), 626–644.

Brito-Neves, B.B., Cordani, U.G., 1991. Tectonic evolution of South America during the Late Proterozoic. Precambrian Res. 53, 23–40.

Burton-Johnson, A., Riley, T.R., 2015. Autochthonous v. accreted terrane development of continental margins: a revised in situ tectonic history of the Antarctic Peninsula. J. Geol. Soc. Lond. https://doi.org/10.1144/jgs2014–1110.

Casquet, C., Herve, F., Pankhurst, R.J., Baldo, E., Calderon, M., Fanning, C.M., Rapela, C.W., Dahlquist, J., 2014. The Mejillonia suspect Terrane (Northern Chile): Late Triassic fast burial and metamorphism of sediments in a magmatic arc environment extending into the Early Jurassic. Gondwana Res. 25, 1272–1286.

Casquet, C., Dahlquist, J.A., Verdecchia, S.O., Baldo, E.G., Galindo, C., Rapela, C.W., Pankhurst, R.J., Morales, M.M., Murra, J.A., Fanning, C.M., 2018. Review of the Cambrian Pampean orogeny of Argentina; a displaced orogeny formerly attached to the Saldania Belt of South Africa? Earth Sci. Rev. 177, 209–225.

Castillo, P., Lacassie, J.P., Augustsson, C., Hervé, F., 2015. Petrography and geochemistry of the Carboniferous–Triassic Trinity Peninsula Group, West Antarctica: implications for provenance and tectonic setting. Geol. Mag. 152 (4), 575–588.

Castillo, P., Fanning, C.M., Hervé, F., Lacassie, J.P., 2016. Characterisation and tracing of Permian magmatism in the south-western segment of the Gondwanan margin; U-Pb age, Lu-Hf and O isotopic compositions of detrital zircons from metasedimentary complexes of northern Antarctic Peninsula and western Patagonia. Gondwana Res. 36, 1–13.

Castillo, P., Fanning, C.M., Pankhurst, R., Hervé, F., Rapela, C., 2017. Zircon O- and Hfisotope constraints on the genesis and tectonic significance of Permian magmatism in Patagonia. J. Geol. Soc. 174 (5), 803–816.

Cawood, P.A., 2005. Terra Australis Orogen: Rodinia breakup and development of the Pacific and Iapetus margins of Gondwana during the Neoproterozoic and Paleozoic. Earth Sci. Rev. 69, 249–279.

Cawood, P.A., Leitch, E.C., Merle, R.E., Nemchin, A.A., 2011. Orogenesis without collision: stabilizing the Terra Australis accretionary orogen, eastern Australia. Geol. Soc. Am. Bull. 123 (11—12), 2240–2255.

Chappell, B.W., White, A.J.R., 1974. Two contrasting granite types. Pac. Geol. 8, 173–174.

Chappell, B.W., White, A.J.R., 1992. I- and S-type granites in the Lachlan Fold Belt. Trans. R. Soc. Edinb. Earth Sci. 83, 1–26.

Charrier, R., 1973. Interruptions of spreading and the compressive tectonic phases of the meridonal Andes. Earth Planet. Sci. Lett. 20, 242–249.

Chelle-Michou, C., Chiaradia, M., Ovtcharova, M., Ulianov, A., Wotzlaw, J.-F., 2014. Zircon petrochronology reveals the temporal link between porphyry systems and the magmatic evolution of their hidden plutonic roots (the Eocene Coroccohuayco deposit, Peru). Lithos 198, 129–140.

Chew, D.M., Schaltegger, U., Košler, J., Whitehouse, M.J., Gutjahr, M., Spikings, R.A., Miškovíc, A., 2007. U-Pb geochronologic evidence for the evolution of the Gondwanan margin of the north-central Andes. Geol. Soc. Am. Bull. 119, 697–711.

Chiaradia, M., Müntener, O., Beate, B., 2011. Enriched basaltic andesites from mid-crustal fractional crystallization, recharge, and assimilation (Pilavo Volcano, Western Cordillera of Ecuador). J. Petrol. 52, 1107–1141.

Clemens, J., Stevens, G., Farina, F., 2011. The enigmatic sources of I-type granites: the peritectic connexion. Lithos 126, 174–181.

Clemens, J.D., 2003. S-type granites — models and evidence. EarthSci. Rev. 61, 1–18.

Cochrane, R., Spikings, R.A., Chew, D., Wotzlaw, J.-F., Chiaradia, M., Tyrell, S., Schaltegger, U., Van der Lelij, R., 2014. High temperature (N350 °C) thermochronology and mechanisms of Pb loss in apatite. Geochim. Cosmochim. Acta 127, 39–56.

Coloma, F., Valin, X., Oliveros, V., Vásquez, P., Creixell, C., Salazar, E., Ducea, M.N., 2017. Geochemistry of Permian to Triassic igneous rocks from northern Chile (28°–29°30′ S): implications on the dynamics of the proto-Andean margin. Andean Geol. 44 (2), 147–178.

Cordani, U.G., Sato, K., 2000. Crustal evolution of the South American platform based on Nd isotopic systematics on granitoid rocks. Episodes 22, 167–173.

D'Abzac, F.-X., Czaja, A.D., Beard, B., Schauer, J.J., Johnson, C.M., 2014. Iron distribution in size-resolved aerosols generated by UV-Femtosecond laser ablation: influence of cell geometry and implications for in situ isotopic determination by LA-MC-ICP-MS. Geostand. Geoanal. Res. 38, 293–309.

Dalziel, I., Elliot, D., 1982. West Antarctica: problem child of Gondwanaland. Tectonics 11 (3), 3–19.

Dalziel, I.W.D., 1984. Tectonic evolution of a fore-arc terrane, southern Scotia Ridge, Antarctica. Geol Soc of America Sp Paper 200, 32 (p).

Dalziel, W.D., 1991. Pacific margins of Laurentia and East Antarctica–Australia as a conjugate rift pair: evidence and implications for an Eocambrian supercontinent. Geology 19, 598–601.

De La Roche, H., Leterrier, J., Grandclaude, P., Marchal, M., 1980. A classification of volcanic and plutonic rocks using R1R2-diagram and major-element analyses - its relationships with current nomenclature. Chem. Geol. 29, 183–210.

Elliot, D.H., 2013. The geological and tectonic evolution of the Transantarctic Mountains: a review. Geol. Soc. Lond. Spec. Publ. 381, 7–35. https://doi.org/10.1144/SP381.14.

Espinoza, M., Montecino, D., Oliveros, V., Astudillo, N., Vasquez, P., Reyes, R., Celis, C., Gonzalez, R., Contreras, J., Creixell, C., Martinez, A., 2019. The synrift phase of the early Domeyko Basin (Triassic, northern Chile): sedimentary, volcanic, and tectonic interplay in the evolution of an ancient subduction-related rift basin. Basin Res. 31, 4–32. https://doi.org/10.1111/bre.12305.

Fanning, C.M., Hervé, F., Pankhurst, R.J., Rapela, C.W., Kleiman, L.E., Yaxley, G.M., Castillo, P., 2011. Lu–Hf isotope evidence for the provenance of Permian detritus in accretionary complexes of western Patagonia and the northern Antarctic Peninsula region. J. S. Am. Earth Sci. 32 (4), 485–496.

Fisher, C.M., Hanchar, J.M., Samson, S.D., Dhuime, B., Blichert-Toft, J., Vervoort, J.D., Lam, R., 2011. Synthetic zircon doped with hafnium and rare earth elements: a reference material for in situ hafnium isotope analysis. Chem. Geol. 286, 32–47.

Flowerdew, M.J., Millar, I.L., Vaughan, A.P.M., Horstwood, M.S.A., Fanning, C.M., 2006. The source of granitic gneisses and migmatites in the Antarctic Peninsula: a combined U-Pb SHRIMP and laser ablation Hf isotope study of complex zircons. Contrib. Mineral. Petrol. 151, 751–768.

Foster, D.A., Gray, D.R., Spaggiari, C.V., Kamenov, G., Bierlein, F.P., 2009. In: Cawood, P.A., Kröner, A. (Eds.), Palaeozoic Lachlan Orogen, Australia; Accretion and Construction of Continental Crust in a Marginal Ocean Setting: Isotopic Evidence from Cambrian Metavolcanic Rocks. Earth Accretionary Systems in Space and Time: The Geological Society, London, Special Publications 318, pp. 329–349.

Franzese, J.R., Spalletti, L.A., 2001. Late Triassic continental extension in southwestern Gondwana: tectonic segmentation and pre-break-up rifting. J. S. Am. Earth Sci. 14, 257–270.

Frost, B.R., Barnes, C.G., Collins, W.J., Arculus, R.J., Ellis, D.J., Frost, C.D., 2001. A geochemical classification of granitic rocks. J. Petrol. 42, 2033–2048. https://doi.org/10.1093/petrology/42.11.2033.

Gao, P., Zheng, Y.F., Zhao, Z.F., 2016. Distinction between S-type and peraluminous I-type granites: zircon versus whole-rock geochemistry. Lithos 258, 77–91.

Gerdes, A., Zeh, A., 2006. Combined U–Pb and Hf isotope LA-(MC-) ICP-MS analyses of detrital zircons: comparison with SHRIMP and new constraints for the provenance and age of an Armorican metasediment in Central Germany. Earth Planet. Sci. Lett. 249, 47–62.

Ghidella, M.E., Yáñez, G., LaBrecque, J.L., 2002. Revised tectonic implications for the magnetic anomalies of the western Weddell Sea. Tectonophysics 347, 65–86.

Golonka, J., Bocharova, N.Y., 2000. Hot spot activity the break-up of Pangea. Palaeogeogr. Palaeoclimatol. Palaeoecol. 161, 49–69.

González, J., Oliveros, V., Creixell, C., Velásquez, R., Vásquez, P., Lucassen, F., 2018. The Triassic magmatism and its relation with the Pre-Andean tectonic evolution: Geochemical and petrographic constrains from the High Andes of north central Chile (29°30′ – 30°S). J. S. Am. Earth Sci. 87, 95–112. https://www.sciencedirect.com/science/article/abs/pii/S0895981117303139.

Goodge, J.W., Fanning, C.M., 2016. Mesoarchean and Paleoproterozoic history of the Nimrod complex, central Transantarctic Mountains, Antarctica: stratigraphic revisions and relation to the Mawson Continent in East Gondwana. Precambrian Res. 285, 242–271. https://doi.org/10.1016/j.precamres.2016.09.001.

Grunow, A.M., Kent, D.V., Dalziel, I.W.D., 1987. Mesozoic evolution of West Antarctica and the Weddell Sea Basin: New paleomagnetic constraints. Earth Planet. Sci. Lett. 86 (1), 16–26. https://doi.org/10.1016/0012-821X(87)90184-1.
Grunow, A.M., Kent, D.V., Dalziel, I.W.D., 1991. New paleomagnetic data from Thurston Island: implications for the tectonics of West Antarctica and Weddell Sea opening. J. Geophys. Res. 96 (17,935-917,954).
Hawkesworth, C.J., Kemp, A.I.S., 2006. Using hafnium and oxygen isotopes in zircons to unravel the record of crustal evolution. Chem. Geol. 226, 144–162.
Helbig, M., Keppie, J.D., Murphy, J.B., Solari, L.A., 2012. U–Pb geochronological constraints on the Triassic–Jurassic Ayu Complex, southern Mexico: derivation from the western margin of Pangea-A. Gondwana Res. 22, 910–927.
Hervé, F., Faúndez, V., Brix, M., Fanning, C.M., 2006a. Jurassic sedimentation of the Miers Bluff Formation, Livingston Island, Antarctica: evidence from SHRIMP U–Pb ages of detrital and plutonic zircons. Antarct. Sci. 18 (2), 229–238.
Hervé, F., Miller, H., Pimpirev, C., 2006b. Patagonia-Antarctic connections before Gondwana break-up. In: Futterer, D., et al. (Eds.), Antarctica: Contributions to Global Earth Sciences. Springer, Berlin, pp. 217–228.
Hervé, F., Calderon, M., Fanning, C.M., Pankhurst, R.J., Fuentes, F., Rapela, C.W., Correa, J., Quezada, P., Marambio, C., 2016. Devonian magmatism in the accretionary complex of southern Chile. J. Geol. Soc. https://doi.org/10.1144/jgs2015-163.
Hoffman, P.F., 1991. Did the breakout of Laurentia turn Gondwaraland inside out? Science 252, 1409–1412.
Hole, M.J., 1988. Post-subduction alkaline volcanism along the Antarctic Peninsula. J. Geol. Soc. Lond. 145, 985–998. https://doi.org/10.1144/gsjgs.145.6.0985.
Jackson, S.E., 2008. Lamtrace data reduction software for LA-ICP-MS. In: Sylvester, P. (Ed.), Laser Ablation ICP-MS in the Earth Sciences: Current Practices and Outstanding Issues. Short Course Series, Vol. 40. Mineralogical Association of Canada, pp. 305–307.
Jacobs, J., Bauer, W., Fanning, C.M., 2003. Late Neoproterozoic/Early Palaeozoic events in central Dronning Maud Land and significance for the southern extension of the East African Orogen into East Antarctica. Precambrian Res. 126, 27–53.
Kay, S.M., Ramos, V.A., Mpodozis, C., Sruoga, P., 1989. Late Paleozoic to Jurassic silicic magmatism at the Gondwana margin: analogy to the Middle Proterozoic in North America? Geology 17, 324–328.
Kemp, A.I.S., Hawkesworth, C.J., Paterson, B.A., Kinny, P.D., 2006. Episodic growth of the Gondwana supercontinent from hafnium and oxygen isotopes in zircon. Nature 439, 580–583.
Kemp, A.I.S., Hawkesworth, C.J., Collins, W.J., Gray, C.M., Blevin, P.L., 2009. Isotopic evidence for rapid continental growth in an extensional accretionary orogen: the Tasmanides, eastern Australia. Earth Planet. Sci. Lett. 284 (3–4), 455–466. https://doi.org/10.1016/j.epsl.2009.05.011.
König, M., Jokat, W., 2006. The Mesozoic breakup of the Weddell Sea. J. Geophys. Res. 111, B12102.
Kula, J.L., Tulloch, A.J., Spell, T.L., Wells, M.L., 2007. Two-stage rifting of Zealandia-Australia-Antarctica: evidence from 40Ar/39Ar thermochronometry of the Sisters shear zone, Stewart Island, New Zealand. Geology 35, 411–414. https://doi.org/10.1130/G23432A.1.
Laudon, T.S., 1991. Petrology of sedimentary rocks from the English Coast, eastern Ellsworth Land. In: Thomson, M.R.A., Crame, J.A., Thomson, J.W. (Eds.), Geological Evolution of Antarctica. Cambridge University Press, Cambridge, pp. 455–460.
Leat, P.T., Scarrow, J.H., Millar, I.L., 1995. On the Antarctic Peninsula batholith. Geol. Mag. 132, 399–4127.
van der Lelij, R., Spikings, R., Gerdes, A., Chiaradia, M., Vennemann, T., Mora, A., 2018. Multi-proxy isotopic tracing of magmatic sources and crustal recycling in the Palaeozoic to Early Jurassic active margin of North-Western Gondwana. Gondwana Res. 66, 227–245.
Litherland, M., Aspden, J., Jemielita, R.A., 1994. The Metamorphic Belts of Ecuador. British Geological Survey. Quito, Overseas Memoir, p. 147.
Ludwig, K.R., 2003. User's Manual for Isoplot 3.00: A Geochronological Toolkit for Microsoft Excel. Kenneth R. Ludwig, Berkeley CA.
Maksaev, V., Munizaga, F., Tassinari, C., 2014. Timing of magmatism of the paleo-Pacific border of Gondwana: U–Pb geochronology of Late Paleozoic to Early Mesozoic igneous rocks of the north Chilean Andes between 20° and 31°S. Andean. Geology 41, 447–506.
Maniar, P.D., Piccoli, P.M., 1989. Tectonic discrimination of granitoids. Geol. Soc. Am. Bull. 101, 635–643. https://doi.org/10.1130/0016-7606(1989)101<0635:TDOG>2.3.CO;2.
Martin, M.W., Clavero, J., Mpodozis, C., 1999. Late Palaeozoic to Early Jurassic tectonic development of the high Andean Principal Cordillera, El Indio region, Chile (29°-30°S). J. S. Am. Earth Sci. 12, 33–49.
Meert, J.G., Lieberman, B.S., 2008. The Neoproterozoic assembly of Gondwana and its relationship to the Ediacaran–Cambrian radiation. Gondwana Res. 14, 5–21. https://doi.org/10.1016/j.gr.2007.06.007.
Meert, J.G., Torsvik, T.H., 2003. The making and unmaking of a supercontinent: Rodinia revisited. Tectonophysics 375, 261–288.
Millar, I.L., Willan, R.C.R., Wareham, C.D., Boyce, A.J., 2001. The role of crustal and mantle sources in the genesis of granitoids of the Antarctic Peninsula and adjacent crustal blocks. J. Geol. Soc. Lond. 158, 855–867.
Millar, I.L., Pankhurst, R.J., Fanning, C.M., 2002. Basement chronology of the Antarctic Peninsula: recurrent magmatism and anatexis in the Palaeozoic Gondwana margin. J. Geol. Soc. Lond. 159, 145–157.
Milne, A.J., Millar, I.L., 1989. The significance of mid-Palaeozoic basement in Graham Land, Antarctic Peninsula. Journal of the Geological Society, London 146, 207–210. https://doi.org/10.1144/gsjgs.146.2.0207.
Mišković, A., Schaltegger, U., 2009. Crustal growth along a non-collisional cratonic margin: a Lu–Hf isotopic survey of the Eastern Cordilleran granitoids of Peru. Earth Planet. Sci. Lett. 279, 303–315.
Mišković, A., Spikings, R.A., Chew, D.M., Kosler, J., Ulianov, A., Schaltegger, U., 2009. Tectonomagmatic evolution of Western Amazonia: geochemical characterization and zircon U–Pb geochronologic constraints from the Peruvian Eastern Cordilleran granitoids. Geol. Soc. Am. Bull. 121, 1298–1324.
Mpodozis, C., Ramos, V., 1989. The Andes of Chile and Argentina. In: Ericksen, G.E., Canas Pinochet, M.T., Reinemund, J.A. (Eds.), Geology of the Andes and its Relation to Hydrocarbon and Mineral Resources. 11. Circum-Pacific Council for Energy and Mineral Resources, Earth Science Series, pp. 59–90.
Navarrete, C., Gianni, G., Encinas, A., Márquez, M., Kamerbeek, Y., Valle, N., Folguera, A., 2019. Upper Triassic to Middle Jurassic geodynamic evolution of southwestern Gondwana: from a large flat-slab to a mantle plume suction in a rollback subduction setting. Earth Sci. Rev. 194, 125–159. https://doi.org/10.1016/j.earscirev.2019. 05.002.
Nelson, D.A., Cottle, J.M., 2017. Long-term geochemical and geodynamic segmentation of the paleo-Pacific margin of Gondwana: insight from the Antarctic and adjacent sectors. Tectonics 36, 3229–3247. https://doi.org/10.1002/2017TC004611.
Nelson, D.A., Cottle, J.M., 2018. The secular development of accretionary orogens: linking the Gondwana magmatic arc record of West Antarctica, Australia and South America. Gonwana Research 63, 15–33. https://doi.org/10.1016/j.gr.2018.06.002.
Oliveros, V., González, J., Espinoza, M., Vásquez, P., Rossel, P., Creixell, C., Sepúlveda, F., Bastías, F., 2017. The early stages of the magmatic arc in the Southern Central Andes. In: Folguera, et al. (Eds.), The Evolution of the Chilean-Argentinean Andes. Springer, Berlín , pp. 185–212. https://link.springer.com/chapter/10.1007/978-3-319-67774-3_7.
Osanai, Y., Nogi, Y., Baba, S., Nakano, N., Adachi, T., Hokada, T., Toyoshima, T., Owada, M., Satish-Kumar, M., Kamei, A., Kitano, I., 2013. Geologic evolution of the Sor Rondane Mountains, East Antarctica: collision tectonics proposed based on metamorphic processes and magnetic anomalies. Precambrian Res. 234, 8–29.
Otamendi, J.E., Ducea, M.N., Bergantz, G.W., 2012. Geological, petrological and geo- chemical evidence for progressive construction of an arc crustal section, Sierra de Valle Fértil, Famatinian arc, Argentina. J. Petrol. 53, 761–800.
Pankhurst, R.J., 1982. Rb-Sr geochronology of Graham Land. J. Geol. Soc. Lond. 139, 701–711.
Pankhurst, R.J., Millar, I.L., Grunow, A.M., Storey, B.C., 1993. The pre-Cenozoic magmatic history of the Thurston Island crustal block, West Antarctica. Journal of Geophysic Research 98, 11835–11849.
Pankhurst, R., Riley, T.R., Fanning, C.M., Kelley, S., 2000. Episodic silicic volcanismin Patagonia and the Antarctic Peninsula: chronology of magmatism associated with the break-up of Gondwana. . J. Petrol. 41, 605–625. https://doi.org/10.1093/petrology/41.5.605.
Pankhurst, R.J., Rapela, C.W., Fanning, C.M., Marquez, M., 2006. Gondwanide continental collision and the origin of Patagonia. Earth Sci. Rev. 76 (3–4), 235–257.
Patchett, J., Tatsumoto, M., 1981. A routine high-precision method for Lu–Hf isotope geochemistry and chronology. Contrib. Mineral. Petrol. 75, 263–267. https://link.springer.com/article/10.1007/BF01166766.
Peacock, M.A., 1931. Classification of igneous rock series. J. Geol. 39, 54–67.
Pearce, J.A., Harris, N.B.W., Tindle, A.G., 1984. Trace element discrimination diagrams for the tectonic interpretation of granitic rocks. J. Petrol. 25, 956–983.
Pin, C., Santos-Zalduegui, J.F., 1997. Sequential separation of light-rare-earth elements, thorium and uranium by miniaturized extraction chromatography: Application to isotopic analyses of silicate rocks. Anal. Chem. Acta. 339, 79–89.
Pindell, J.L., Tabbutt, K.D., 1995. Mesozoic–Cenozoic Andean Paleogeography and regional controls on hydrocarbon systems. In: Tankard, A.J., Suarez, R., Welsink, H.J. (Eds.), Petroleum Basins of South America. 62. American Association of Petroleum Geologists Memoir, pp. 101–128.
Ramos, V.A., 1994. Terranes of Southern Gondwanaland and their control in the Andean Structure (30°–33°S latitude). In: Reutter, K.-J., Scheuber, E., Wigger, P.J. (Eds.), Tectonics of the Southern Central Andes. Springer-Verlag, Heidelberg, pp. 249–261.
Ramos, V.A., 2008. Patagonia: a paleozoic continent adrift? J. S. Am. Earth Sci. 26, 235–251.
Ramos, V.A., Kay, S.M., 1991. Triassic rifting and associated basalts in the Cuyo basin, central Argentina. Geol. Soc. Am. Spec. Pap. 265, 79–92.
Riley, T., Leat, P., Pankhurst, R., Harris, C., 2001. . Origins of large volume rhyolitic volcanism in the Antarctic Peninsula and Patagonia by crustal melting. J. Petrol. 42, 1043–1065. https://doi.org/10.1093/petrology/42.6.1043.
Ramos, V.A., 2009. Anatomy and global context of the Andes: main geologic features and the Andean orogenic cycle. Geol. Soc. Am. Mem. 204, 31–65.
Ramos, V.A., Naipauer, M., 2014. Patagonia: where does it come from? J. Iber. Geol. 40, 367–379.
Rapela, C., Pankhurst, R., Casquet, C., Dahlquist, J., Fanning, M., Baldo, E., Galindo, C., Alasino, P., Ramacciotti, C., Verdecchia, S., Murra, J., Basei, M., 2018. A review of the Famatinian Ordovician magmatism in southern South America: evidence of lithosphere reworking and continental subduction in the early proto-Andean margin of Gondwana. Earth Sci. Rev. https://doi.org/10.1016/j.earscirev.2018.10.006.
del Rey, Á., Deckart, K., Arriagada, C., Martínez, F., 2016. Resolving the paradigm of the late Paleozoic–Triassic Chilean magmatism: isotopic approach. Gondwana Res. 37, 172–181. https://doi.org/10.1016/j.gr.2016.06.008.
del Rey, Á., Deckart, K., Planavsky, N., Arriagada, C., Martinez, F., 2019. Tectonic evolution of the southwestern margin of Pangea and its global implications: evidence from the mid Permian–Triassic magmatism along the Chilean-Argentine border. Gondwana Res. 76 (2019), 303–321. https://doi.org/10.1016/j.gr.2019.05.007.
Rezeau, H., Moritz, R., Wotzlaw, J.F., Tayan, R., Melkonyan, R., Ulianov, A., Selby, D., d'Abzac, F.X., Stern, R.A., 2016. Temporal and genetic link between incremental pluton assembly and pulsed porphyry Cu-Mo formation in accretionary orogens. Geology 44 (8), 627–630.
Riley, T.R., Flowerdew, M.J., Whitehouse, M.J., 2012a. U–Pb ion-microprobe zircon geochronology from the basement inliers of eastern Graham Land, Antarctic Peninsula.

Journal of the Geological Society, London 169, 381–393. https://doi.org/10.1144/0016-76492011-142.
Riley, T.R., Flowerdew, M.J., Whitehouse, M.J., 2012b. Chrono- and lithostratigraphy of a Mesozoic–Tertiary fore- to intra-arc basin: Adelaide Island, Antarctic Peninsula. Geol. Mag. 149, 768–782.
Riley, T.R., Flowerdew, M.J., Pankhurst, R.J., Curtis, M.L., Millar, I.L., Fanning, C.M., Whitehouse, M.J., 2017a. Early Jurassic magmatism on the Antarctic Peninsula and potential correlation with the Subcordilleran plutonic belt of Patagonia. J. Geol. Soc. Lond. 174 (2), 365–376. https://doi.org/10.1144/jgs2016-053.
Riley, T.R., Flowerdew, M.J., Pankhurst, R.J., Millar, I.L., Leat, P.T., Fanning, C.M., Whitehouse, M.J., 2017b. A revised geochronology of Thurston Island, West Antarctica, and correlations along the proto-Pacific margin of Gondwana. Antarct. Sci. 29, 47–60. https://doi.org/10.1017/S0954102016000341.
https://www.cambridge.org/core/journals/antarctic-science/article/antarctic-peninsula-granitoid-petrogenesis-a-case-study-from-mount-charity-northeastern-palmer-land/C1E9E94265861866ADF796D7EEE0A8B9
Scarrow, J., Leat, P., Wareham, C.D., Millar, I., 1998. Geochemistry of mafic dykes in the Antarctic Peninsula continental-margin batholith: a record of arc evolution. Contrib. Mineral. Petrol. 289–305.
Scott, J.M., Cooper, A.F., Palin, J.M., Tulloch, A.J., Kula, J., Jongens, R., Spell, T.L., Pearson, N.J., 2009. Tracking the influence of a continental margin on growth of a magmatic arc, Fiordland, New Zealand, using thermobarometry, thermochronology, and zircon U–Pb and Hf isotopes. Tectonics 28. https://doi.org/10.1029/2009tcc002489 (20 pp).
Slama, J., Košler, J., Condon, D.J., Crowley, J.L., Gerdes, A., Hanchar, J.M., Horstwood, M.S.A., Morris, G.A., Nasdala, L., Norberg, N., Schaltegger, U., Schoene, B., Tubrett, M.N., Whitehouse, M.J., 2008. Plešovice zircon — a new natural reference material for U–Pb and Hf isotopic microanalysis. Chem. Geol. 249 (1–2), 1–35.
Smellie, J.L., 1991. Stratigraphy, provenance and tectonic setting of (?) Late Palaeozoic–Triassic sedimentary sequences in northern Graham Land and South Scotia Ridge. In: Thomson, M.R.A., Crame, J.A., Thomson, J.W. (Eds.), Geological Evolution of Antarctica. Cambridge University Press, Cambridge, pp. 411–417.
Söderlund, U., Patchett, J., Vervoort, J., Isachsen, C., 2004. The 176Lu decay constant determined by Lu–Hf and U–Pb isotope systematics of Precambrian mafic intrusions. Earth Planet. Sci. Lett. 219, 311–324.
Spikings, R., Cochrane, R., Villagomez, D., Van der Lelij, R., Vallejo, C., Winkler, W., Beate, B., 2015. The geological history of northwestern South America: from Pangaea to the early collision of the Caribbean Large Igneous Province (290–75 Ma). Gondwana Res. 27, 95–139.
Spikings, R., Rietsma, M., Boekhout, F., Mišković, A., Ulianov, A., Chiaradia, M., Gerdes, A., Schaltegger, U., 2016. Characterisation of Triassic rifting in Peru and implications for the early disassembly of western Pangaea. Gondwana Res. 35, 124–143.
Storey, B., Garrett, S., 1985. Crustal growth of the Antarctic Peninsula by accretion, magmatism and extension. Geol. Mag. 122, 5–14.
Storey, B.C., Dalziel, I.W.D., Garrett, S.W., Grunow, A.M., Pankhurst, R.J., Vennum, W.R., 1998. West Antarctica in Gondwanaland: crustal blocks, reconstruction and breakup processes. Tectonophysics 155, 381–390.
Suarez, M., 1976. Plate-tectonic model for southern Antarctic Peninsula and its relation to southern Andes. Geology 4, 211–214.
Suarez, R., Gonzalez, P., Ghiglione, M., 2019. A review on the tectonic evolution of the Paleozoic-Triassic basins from Patagonia: Record of protracted westward migration of the pre-Jurassic subduction zone. J. S. Am. Earth Sci. 95, 102256. https://doi.org/10.1016/j.jsames.2019.102256.
Sun, S.S., McDonough, W.F., 1989. Chemical and isotopic systematics of oceanic basalts: implications for mantle composition and processes. In: Saunders, A.D., Norry, M.J. (Eds.), Magmatism in Ocean Basins. Geologogical Society of London Special Publication 42, pp. 313–345.
Tanaka, T., et al., 2000. JNdi-1: a neodymium isotopic reference in consistency with La Jolla neodymium. Chem. Geol. 168, 279–281.
Tangeman, J.E., Mukasa, S.B., Grunow, A.M., 1996. Zircon U–Pb geochronology of plutonic rocks from the Antarctic Peninsula: confirmation of the presence of unexposed Paleozoic crust. Tectonics 15, 1309–1324.
Taylor, S.R., McLennan, S.M., 1995. The geochemical evolution of the continental crust. Rev. Geophys. 33, 241–265.
Thirlwall, M.F., Anczkiewicz, R., 2004. Multidynamic isotope ratio analysis using MC-ICP-MS and the causes of secular drift in Hf, Nd and Pb isotope ratios. Int. J. Mass Spectrom. 235, 59–81.
Thomson, M.R.A., 1975. First marine Triassic fauna from the Antarctic Peninsula. Nature 257, 577–578.
Ulianov, A., Muntener, O., Schaltegger, U., Bussy, F., 2012. The data treatment dependant variability of U–Pb zircon ages obtained using mono-collector, sector field, laser ablation ICP-MS. J. Anal. At. Spectrom. 27, 663–676.
Villagómez, D., Spikings, R., Magna, T., Kammer, A., Winkler, W., Beltrán, A., 2011. Geochronology, geochemistry and tectonic evolution of the Western and Central cordilleras of Colombia. Lithos 125, 875–896.
Vervoort, J.D., Patchett, P.J., 1996. Behaviour of hafnium and neodymium isotopes in the crust: constraints from Precambrian crustally derived granites. Geochim. Cosmochim 60, 3717–3733.
Valley, J.W., Graham, C.M., Harte, B., Eiler, J.M., Kinney, P.D., 1998. Ion microprobe analysis of oxygen, carbon and hydrogen isotope ratios. In: McKibben, M.A., Shanks, W.C., III, W.I. Ridley (Eds.), Applications of Microanalytical Techniques to Understanding Mineralizing Processes. 7. Society of Economic Geologists, pp. 73–98.
Valley, J.W., Lackey, J.S., Cavosie, A.J., Clechenko, C.C., Spicuzza, M.J., Basei, M.A.S., Bindeman, I.N., Ferreira, V.P., Sial, A.N., King, E.M., Peck, W.H., Sinha, A.K., Wei, C.S., 2005. 4.4 billion years of crustal maturation: oxygen isotope ratios of magmatic zircon. Contrib. Mineral. Petrol. 150 (6), 561–580.
Vasquez, P., Glodny, J., Franz, G., Frei, D., Romer, R.L., 2011. Early Mesozoic plutonism of the Cordillera de la Costa (34-37S), Chile. Constraints on the onset of the Andean orogeny. J. Geol. 119, 159–184.
Vaughan, A.P.M., Storey, B.C., 2000. The eastern Palmer Land shear zone: a new terrane accretion model for the Mesozoic development of the Antarctic Peninsula. J. Geol. Soc. Lond. 157, 1243–1256. https://doi.org/10.1144/jgs.157.6.1243.
Vaughan, A.P.M., Eagles, G., Flowerdew, M.J., 2012a. Evidence for a two-phase Palmer Land event from crosscutting structural relationships and emplacement timing of the Lassiter Coast Intrusive Suite, Antarctic Peninsula: implications for mid-Cretaceous Southern Ocean plate configuration. Tectonics 31, TC1010.
Vaughan, A.P.M., Leat, P.T., Dean, A.A., Millar, I.L., 2012b. Crustal thickening along the West Antarctic Gondwana margin during mid-cretaceous deformation of the Triassic intra-oceanic Dyer Arc. Lithos 142–143, 130–147. https://doi.org/10.1016/j.lithos.2012.03.008.
Veevers, J.J., Tewari, R.C., 1995. Permian–Carboniferous and Permian–Triassic magmatism in the rift zone bordering the Tethyan margin of southern Pangea. Geology 23, 467–470.
Vervoort, J.D., Patchett, P.J., Blichert-Toft, J., Albarède, F., 1999. Relationships between Lu–Hf and Sm–Nd isotopic systems in the global sedimentary system. Earth Planet. Sci. Lett. 168, 79–99.
Wever, H.E., Millar, I.L., Pankhurst, R.J., 1994. Geochronology and radiogenic isotope geology of Mesozoic rocks from eastern Palmer Land, Antarctic Peninsula: Crustal anatexis in arc-related granitoid genesis. J. S. Am. Earth Sci. 7, 69–83.
Wever, H.E., Storey, B.C., Leat, P.T., 1995. Peraluminous granites in NE Palmer Land, Antarctic Peninsula; early Mesozoic crustal melting in a magmatic arc. J. Geol. Soc. Lond. 152, 85–96.
Wiedenbeck, M., Alle, P., Corfu, F., Griffin, W.L., Meier, M., Oberli, F., von Quadt, A., Roddick, J.C., Spiegel, W., 1995. 3 natural zircon standards for U-Th-Pb, Lu-Hf, trace-element and REE analyses. Geostand. Newslett. 19, 1–23.
Zen, E., 1988. Phase relations of peraluminous granitic rocks and their petrogenetic implications. Annu. Rev. Earth Planet. Sci. 16, 21–51.
Zindler, A., Hart, S., 1986. Chemical Geodynamics. Annu. Rev. Earth Planet. Sci. 14, 493–571.